# Molecular Dynamics Study of CO2 and H2O Intercalation in Smectite Clays: Effect of Temperature and Pressure on Interlayer Structure and Dynamics in Hectorite

Narasimhan Loganathan, A. Ozgur Yazaydin, Geoffrey M. Bowers, Andrey G. Kalinichev, R. James Kirkpatrick

THE JOURNAL OF PHYSICAL CHEMISTRY C

Article

# Molecular Dynamics Study of CO and HO Intercalation in Smectite Clays: Effect of Temperature and Pressure on Interlayer Structure and Dynamics in Hectorite

Narasimhan Loganathan, A. Ozgur Yazaydin, Geoffrey M Bowers, Andrey G. Kalinichev, and R. James Kirkpatrick

*J. Phys. Chem. C*, **Just Accepted Manuscript** • DOI: 10.1021/acs.jpcc.7b06825 • Publication Date (Web): 11 Oct 2017



ACS Publications

The Journal of Physical Chemistry C is published by the American Chemical Society. 1155 Sixteenth Street N.W., Washington, DC 20036

# Molecular Dynamics Study of $CO_2$ and $H_2O$ Intercalation in Smectite Clays: Effect of Temperature and Pressure on Interlayer Structure and Dynamics in Hectorite

*Narasimhan Loganathan[1], A. Ozgur Yazaydin[1,2],[*] Geoffrey M. Bowers[3], Andrey G. Kalinichev[4] and R. James Kirkpatrick[5]*

[1] Department of Chemistry, Michigan State University, East Lansing, Michigan 48824, United States

[2] Department of Chemical Engineering, University College London, London, WC1E7JE, United Kingdom

[3] Department of Chemistry and Biochemistry, St. Mary's College of Maryland, St. Mary's City, Maryland 20686, United States

[4] Laboratoire SUBATECH (UMR-6457), Institut Mines-Télécom Atlantique, F-44307, Nantes, France

[5] College of Natural Science, Michigan State University, East Lansing, Michigan 48824, United States

[*] **Corresponding author e-mail: ozgur.yazaydin@ucl.ac.uk**

## ABSTRACT

Grand Canonical Molecular Dynamics (GCMD) simulations were performed to investigate the intercalation of $CO_2$ and $H_2O$ molecules in the interlayers of the smectite clay, Na-hectorite, at temperatures and pressures relevant to petroleum reservoir and geological carbon sequestration conditions and in equilibrium with $H_2O$-saturated $CO_2$. The computed adsorption isotherms indicate that $CO_2$ molecules enter the interlayer space of Na-hectorite only when it is hydrated with approximately 3 $H_2O$ molecules per unit cell. The computed immersion energies show that the bilayer hydrate structure (2WL) contains less $CO_2$ than the monolayer structure (1WL), but that the 2WL hydrate is the most thermodynamically stable state, consistent with experimental results for a similar Na-montmorillonite smectite. At all *T* and *P* conditions examined (323-368 K and 90-150 bar), the $CO_2$ molecules are adsorbed at the midplane of clay interlayers for the 1WL structure and closer to one of the basal surfaces for the 2WL structure. Interlayer $CO_2$ molecules are dynamically less restricted in the 2WL structures. The $CO_2$ molecules are preferentially located near basal surface oxygen atoms and $H_2O$ molecules rather than in coordination with $Na^+$ ions. Accounting for the orientation and flexibility of the structural -OH groups of the clay layer has a significant effect on the details of the computed structure and dynamics of $H_2O$ and $CO_2$ molecules but does not affect the overall trends with changing basal spacing or the principal structural and dynamical conclusions. Temperature and pressure in the ranges examined have little effect on the principal structural and energetic conclusions, but the rates of dynamical processes increase with increasing temperature, as expected.

## INTRODUCTION

The interaction of $CO_2$ with clay minerals is important in controlling the behavior of $CO_2$ in the geological subsurface and has gained increasing research interest due to its potential importance in enhanced oil recovery, shale gas exploration, and geologic sequestration strategies for mitigating atmospheric $CO_2$.[1-3] After injection, $CO_2$ can change the pH of the aqueous pore fluid, potentially causing dissolution of some mineral phases. $CO_2$ can also be trapped by cap rocks typically containing a large fraction of clay minerals.[4-10] Thus, successful, long term confinement of $CO_2$ depends on its interaction with the clays of the cap rocks. Several recent studies have focused on the interaction of $CO_2$ with clay minerals, particularly its intercalation in smectite interlayers.[11-22] In geological carbon sequestration or $CO_2$ flooding, supercritical carbon dioxide (*sc*$CO_2$, $T_c$~31ºC, $P_c$~73 bar) is injected underground, where it can interact with the resident $H_2O$-rich pore fluid and dissolved, surface and interlayer-adsorbed ions. Under these conditions, $CO_2$ can penetrate into hydrated smectite interlayers which would then expand or contract depending on a variety of factors, including the thermodynamic $H_2O$ activity and the interlayer cations present.[12, 16-22] Numerous experimental and computational studies have shown that the structure and dynamics of fluids confined in smectite interlayers are different than on external clay surfaces or in bulk solution.[23-37] Importantly, the swelling characteristics depend on the nature of the charge balancing metal cations (characterized by their hydration energy and polarizability), the smectite composition, and the location of the structural charge.[29,31,33,38,39] Hence, it is essential to have a better molecular-scale understanding of the structure and dynamics of intercalated $H_2O$ and $CO_2$ molecules at temperature and pressure conditions relevant to petroleum reservoirs and geological carbon sequestration.

Our previous experimental NMR and computational molecular modeling studies of hydrated hectorite have shown good agreement in the ion adsorption, swelling behavior, and structural and dynamic characteristics with experimental and molecular simulation studies of similar hydrated montmorillonite interlayers.[7,11,25,27-29,31,33,34,36-38,40-42] Both montmorillonite and hectorite develop their structural charge in the octahedral sheet, and we expect the results here to be in good agreement. We use hectorite here to allow direct comparison with our earlier NMR results for that phase. NMR studies with natural montmorillonites typically yield poorly resolved spectra due to paramagnetic effects resulting from their relatively high Fe contents. In contrast, very low-Fe are available in hectorite makes it a very good model smectite clay.

The intercalation of $CO_2$ in smectite interlayers has been successfully probed *in situ* using advanced X-ray diffraction (XRD), infrared (IR) and nuclear magnetic resonance (NMR) experiments at elevated temperatures and $CO_2$ pressures[11-14,16-18,20,22,43-46] For example, XRD studies by Giesting et al.[14,17,18] and Schaef et al.[19,20,22] showed that the interlayer expansion or shrinkage of $Na^+$-, $Ca^{2+}$- and $Mg^{2+}$-montmorillonite is determined by the extent of water saturation in the *sc*$CO_2$ fluid phase. Most importantly, these studies indicate that with those cations present, $CO_2$ enters the interlayer only if there is at least a sub-monolayer of $H_2O$ present. The results of Loring et al.[43,44,46] reinforce the same view of the intercalation mechanism in Na-montmorillonite. These studies indicated that the maximum extent of $CO_2$ intercalation in Na-montmorillonite at 323 K and 90 bar occurs when the interlayer $H_2O$ content corresponds to that of a monolayer hydrate state (1WL). Recent NMR investigation of $CO_2$ in hectorite by Bowers et al.[12] demonstrate the importance of the charge balancing cation in understanding the intercalation of $CO_2$ and the dynamics of interlayer $CO_2$ molecules. For instance, these authors have reported greater $CO_2$ intercalation in Cs-hectorite compared to Na- and Ca-hectorite. In addition, despite

the similar ionic radii of $Ca^{2+}$ and $Na^{+}$, Ca-hectorite incorporates more $CO_2$ than Na-hectorite, probably due to the smaller number of $Ca^{2+}$ ions present in the interlayer. This result is consistent with previous studies on other smectites.[28,31,33] As the $H_2O$ activity of the $CO_2$-rich fluid increases, $Na^{+}$ and $Ca^{2+}$ hectorites expand and adsorb progressively more $H_2O$ and less $CO_2$, whereas Cs-hectorite maintains a constant basal spacing with an increasing interlayer $H_2O/CO_2$ ratio. For all three phases, some interlayer $CO_2$ is present at all $H_2O$ activities, with Cs-hectorite incorporating the most $CO_2$ at all conditions between anhydrous and $H_2O$ saturation. In addition, changes in the $H_2O$ activity of the bulk fluid phase alter the structure and dynamics in the interlayers and on the external surfaces of clay particles.[12,20,44] These recent results highlight the importance of having detailed information about the interlayer $CO_2/H_2O$ partitioning and the molecular scale structural and dynamical interplay between these species in smectite clays under *T* and *P* conditions relevant to petroleum reservoirs and geological carbon sequestration.

Computational modeling studies using molecular dynamics (MD) and Monte Carlo (MC) methods are making significant contributions to characterize the nano-confinement of $CO_2$ - $H_2O$ binary mixtures in layered structured materials.[47-53] Makaremi et al.[48] used Gibbs Ensemble Monte Carlo (GEMC) simulations with both $H_2O$-rich and $CO_2$-rich fluids at 348 K and 125 bars and found the swelling behavior to be strongly dependent on the location of the structural charge sites. Despite having the same structural charge, Na-montmorillonite with only octahedral charge exhibits stable 1WL (12.5 Å) and 2WL (15.5 Å) hydration states, whereas Na-beidellite with only tetrahedral charge is stable only as a 1WL structure with a 12.5 Å basal spacing.[48] Botan et al.[51] reported a stable 2WL (15.3Å) structure for Na-montmorillonite with only octahedral charge in contact with a fluid composition corresponding to water saturated $CO_2$ at 348 K and 125 bar using Grand Canonical Monte Carlo (GCMC) simulations. They reported

that the mole fraction of $CO_2$ in the interlayer reaches a maximum at 1WL basal spacings (12.4 Å) and decreases gradually at larger spacings, consistent with later experimental studies.[43,44] Recently, Rao et al.[50] performed simulations using GCMC methods that illustrated the importance of small differences in structural charge (-0.8|*e*| *vs* -1.0|*e*|) on the interlayer $CO_2$ mole fraction at 323 K and 90 bar for Na-montmorillonite. This study suggests that higher structural charge leads to decreased interlayer $CO_2$ at all water activities. These MC simulations yield computed interlayer $CO_2$ mole fractions that agree reasonably well with experimental results for Na-montmorillonite.[43,44] They do not, however, provide structural and dynamical information about the intercalated species, because of the stochastic nature of the MC method. This information is usually obtained by classical MD simulations performed on the equilibrium structures of stable states determined by MC procedures at the same *T* and *P* conditions.[48-51] These MD results have shown that regardless of the structural charge and its location, in Na-montmorillonite $CO_2$ molecules are located at the middle of the interlayer gallery at 1WL basal spacings but close to one of the basal surfaces at 2WL basal spacings.[51] However, the structural environments of interlayer $CO_2$ molecules have not been sufficiently investigated, and there is little information about how their dynamical behavior changes with hydration and interlayer expansion.

This paper uses a computational Grand Canonical Molecular Dynamics (GCMD) approach to examine the intercalation and dynamics of $H_2O$ and $CO_2$ molecules in the smectite mineral hectorite in equilibrium with a binary $CO_2$-rich, $H_2O$-saturated fluid. Our approach incorporates GCMC and MD procedures, allowing for determination of adsorption and structural and dynamical details using the same simulation run. One important advantage is that layer displacement to obtain the equilibrium interlayer distribution of the intercalated species is

performed by the MD procedure instead of involving a regular MC step. The GCMD method was previously used to study the hydration of Cs-montmorillonite in equilibrium with pure $H_2O$ and showed results in good agreement with experiment.[54] To our knowledge, GCMD methods have not previously been used to study intercalation of binary fluid mixtures in layered-structure materials.

We performed calculations for nine temperature and pressure combinations relevant to petroleum reservoir and geological carbon sequestration conditions at basal spacings from 9.5 to 18.0 Å to provide changes in interlayer $CO_2/H_2O$ ratios, the structural environments and the orientations of intercalated molecules, and their dynamical behavior. The role of the orientation of the structural ($OH^-$) groups to determine the interlayer $CO_2$ mole fraction is reported. The relationship between the different coordination environments and the dynamics of interlayer species is in good agreement with previous experimental and MC and MD simulation studies of hectorite and montmorillonite.[12,28,43-45,48-52]

## SIMULATION DETAILS

Hectorite is a 2:1 trioctahedral smectite clay with a sheet of octahedrally coordinated cations sandwiched between two sheets of $SiO_4$ tetrahedra that share three vertices with other silicate tetrahedra. Isomorphic substitution of $Li^+$ for $Mg^{2+}$ in the octahedral sheet results in a net negative structural charge that is compensated by interlayer cations. The structural formula of our hectorite simulation model is $M^+(Mg_5Li)Si_8O_{20}(OH)_4$, and the structure is based on that of Breu et al.[55] but with (OH) substituted for F. This model exhibits characteristics quite similar to the natural San Bernardino hectorite used in our experimental studies, except that the model contains only hydroxyl groups on the octahedral sheet rather than the mix of F-/OH- in the

natural hectorite.[7,11,12,23,25,27,29,36] The hydration behavior of synthetic fluoro-hectorite has been discussed previously.[26,56]

The simulation supercell consisted of 16 crystallographic unit cells of hectorite (4 × 2 × 2) encompassing two interlayers. The lateral dimensions of the simulated model are ~ 20 Å × 18 Å and are sufficiently large to avoid finite size effects. This supercell size allows for a quasi-disordered distribution of $Li^{+}/Mg^{2+}$ isomorphic substitutions in the octahedral sheet (in accordance with Loewenstein's rule[57]) and thus of the associated structural charge (see Figure 1 in ref. 31). The distribution of isomorphic substitutions was imposed only after the unit cell was replicated in all crystallographic directions to form the supercell. This procedure yields a hectorite model in which each layer has a different arrangement of $Li^{+}$ ions in the octahedral sheet. Details of the hectorite structure are described elsewhere.[28,31,33,53]

We performed GCMD[58] simulations in the grand canonical ensemble for Na-hectorite at nine temperature ($T$) and pressure ($P$) combinations relevant to reservoir and sequestration conditions (Table 1). The interlayer spacings were varied from 9.5 Å to 18.0 Å at steps of 0.2 Å. Each interlayer in a given model was constrained to have the same $z$-spacing dimension, which was held constant throughout the run. However, the T-O-T layers were allowed to move laterally (along $x$ and $y$) during the MD simulation without disrupting the structure. This lateral movement is essential for proper calculation of the structure, dynamics, and energetics, because the minimum energy positions of the two layers in the $x$-$y$ plane across an interlayer vary with the cation and the number of intercalated fluid molecules.[40,41,51] Two sets of simulations were performed that differed in the flexibility of the structural –OH groups. In one set, the relative positions of all the atoms in a given layer were fixed except for the H-atoms of the OH groups, for which the (Mg/Li)-O-H angle was allowed to vary during the simulation. In the other set, the

relative positions of all atoms in the layers, including the structural OH groups, were fixed with the O-H vector perpendicular to the basal surfaces throughout the simulation. Hence, the T-O-T layers with unrestricted OH groups are called "flexible" whereas those with fixed OH groups as "rigid" when discussing the results.

The hybrid GCMD approach incorporates MC and MD procedures by MC sampling of the insertion and deletion of fluid molecules with equal probability at each MD time step. Therefore, in the GCMD simulations, the number of interlayer molecules fluctuates, but the temperature, volume of the simulation cell, and chemical potential of the reservoir fluid components are fixed. A modified version of the RASPA simulation package was used to perform the simulations.[59] The interatomic interactions for the substrate species (hectorite and cations) were calculated with the ClayFF force field,[60] which is used widely in molecular simulations of clays and other silicate materials. The $H_2O$ and $CO_2$ molecules were held rigid and were represented by the SPC[61] and EPM2[62] models, respectively. Ewald summation was used for computing the long-range electrostatic interactions with an accuracy of $10^{-6}$.[63] A Nosé-Hoover thermostat controlled temperature,[64] and three-dimensional periodic boundary conditions were employed with a cutoff of 9.0 Å for short range non-electrostatic interactions. The MD time step was 1 fs. The reservoir compositions of the bulk $H_2O$-$CO_2$ fluids correspond to an $H_2O$-saturated $CO_2$-rich phase at each pressure and temperature. The values were obtained from the experimental solubility data of Spycher et al.[65] and are different for each *T* and *P* combination (Table 1). The acceptance and rejection rules of the insertion/deletion moves require the fugacities of both fluid species (Table 1), which were obtained from the Peng-Robinson equation of state.[66] This equation of state was shown to yield satisfactory results for $H_2O$-$CO_2$ fluids at the range of *T* and *P* values investigated.[65] For each modeled system, the GCMD simulations were

performed for 15 ns to attain equilibration, followed by another 15 ns for the production run. The adsorption isotherms and related structure, dynamics, and energetics were calculated from the last 5 ns of the equilibrium production run. The reported values of the calculated parameters are the means of the values for five time blocks of 1 ns each.

The interlayer energetics and adsorption profiles of the hectorite with intercalated $CO_2$ and $H_2O$ were analyzed quantitatively. The energetic approach used here is similar to that of Smith,[42] which is widely used for swelling clays.[28,31,33,37] The change in energy due to $H_2O$ and $CO_2$ adsorption with varying basal spacing is characterized by the immersion energy, $Q$, which is given by

$$Q = \langle U(N) \rangle - \langle U(N_{\mathrm{ref}}) \rangle - ((N - N_{\mathrm{H2O-ref}})U_{\mathrm{H2O-bulk}} + (N - N_{\mathrm{CO2-ref}})U_{\mathrm{CO2-bulk}}) \quad (1)$$

where $N_{\mathrm{H2O-ref}}$, $N_{\mathrm{CO2-ref}}$ and $\langle U(N_{\mathrm{ref}}) \rangle$ correspond to the number of $H_2O$ and $CO_2$ in the interlayer and the average potential energy of a reference state. Here, the largest basal spacing (18.0 Å) is the reference state, because its potential energy is closest to the bulk value in comparison to those at other basal spacings.[42]

Structural properties at different basal spacings were analyzed by computing the atomic density distributions of all interlayer species. The orientation distributions of the intercalated molecules were evaluated using the angles between the normal to the basal surface and the $H_2O$ dipole, H-H vector ($H_2O$), and O-C-O vector ($CO_2$). The impact of intercalated $CO_2$ molecules on the interlayer H-bonding network was evaluated using the commonly applied geometric criteria of H-bonding, where an H-bond is assumed to exist if, and only if, the intermolecular O···H distance is < 2.45 Å and the angle between the O···O and O-H vectors is < 30°.[67-69] For

H-bond analysis, the O atoms of the basal surface, $O_b$, and the O atoms of the $CO_2$, $O_{CO2}$, were considered to be potential H-bond acceptors like the O atoms of the $H_2O$, $O_{H2O}$.

The dynamical properties of the intercalated $H_2O$, $CO_2$, and $Na^+$ ions were determined by computing the residence times for nearest neighbor (NN) coordination of the $O_b$, $Na^+$, and $O_{H2O}$ and $O_{CO2}$. The average residence times for different atomic pairs were determined by time correlation functions similar to those describing H-bond lifetimes.[70-72] Intermittent and continuous residence times were calculated. To define the intermittent residence time, the correlation function $c(t)$ is given a value of 1 when pairs of atoms are within the first coordination sphere, and 0 otherwise. However, the pair is considered coordinated if their coordination is lost and then re-established later in the simulation. In contrast, the continuous residence time correlation function, $C(t)$, is defined similarly, except re-entries are not considered as coordinated if the coordination between a certain pair is lost for a short time. A time interval of 2 ps was used for computing these averages. This period is comparable to the residence times of $H_2O$ in hydration shells of ions, as determined in earlier studies.[31,33,73] Detailed descriptions of these residence time correlation functions and their analysis is discussed elsewhere.[31,33,34]

## RESULTS AND DISCUSSION

### Adsorption Isotherm and Energetics

Overall, the computed intercalation behavior of $H_2O$ and $CO_2$ is the same in the simulations with flexible and rigid structural OH groups over the range of $T$ and $P$ studied (Figures 1a-1d). No intercalation occurs at basal spacings of <10.2 Å. $H_2O$ intercalation occurs at ~10.3 Å and increases with increasing basal spacing. $CO_2$ intercalation occurs beginning at

~11.2 Å, increases to 12.2 Å (flexible) or 12.5 Å (rigid), and decreases at larger spacings. Basal spacings less than the 1WL values of 12.2 Å or 12.5 Å correspond to a partial 1WL structure, and the values near 15.2Å indicate 2WL structures. The computed adsorption characteristics are consistent with recent high-*T* and *P* XRD and IR studies,[12,14,18,43,44] which show that a small number of interlayer $H_2O$ in smectite interlayers promotes $CO_2$ intercalation. Adsorption character is in good agreement with experimental studies that suggest that the maximum intercalation of $CO_2$ occurs at basal spacings corresponding to a 1WL hydrate[12,14,17,18-21,43] and with MC simulations on montmorillonite that show similar results.[48-51]

At all basal spacings and for all *T*-*P* conditions studied, however, the mole fractions of adsorbed $H_2O$ and $CO_2$ in the interlayer are quantitatively different with flexible and rigid –OH groups. Simulations using flexible –OH groups show fewer intercalated $CO_2$ molecules and more $H_2O$ molecules compared to those with rigid –OH groups. Importantly, at distances > 15.0 Å, few $CO_2$ molecules are adsorbed with flexible –OH groups, and at basal spacings > 16.0 Å there is no interlayer $CO_2$ (Figures 1a-1c). In contrast, with rigid –OH groups $CO_2$ adsorption reaches a plateau (Figure 1d) at these basal spacings. The larger number of intercalated $CO_2$ molecules with rigid –OH groups is compensated by fewer $H_2O$ molecules at all basal spacings (Table 2). However, with both flexible and rigid -OH groups, varying temperature in the simulated range (323-368 K) has little effect on the intercalation, and with the flexible -OH groups varying pressure in the 90 – 150 bar range also has little effect (Figures 1a-1d). The quantitative differences in the $CO_2$ and $H_2O$ intercalation with the flexible and rigid –OH groups is due to decreased electrostatic interaction between the clay surface and $Na^+$ ions in the latter case with the orientations of the -OH groups fixed in their crystallographic positions perpendicular to the basal surface. This decreased electrostatic attraction makes $Na^+$ less strongly adsorbed to the clay

surface, leading to stronger $Na^+$-$H_2O$ and $H_2O/CO_2$-surface association. This structural arrangement allows increased $CO_2$ adsorption due to the relatively larger volumetric space available for $CO_2$ coordination with the basal surface sites that with flexible –OH groups are occupied by $Na^+$ ions. Because flexible -OH groups are a more realistic representation of the physical behavior of clays, these results show that they should be used in future simulations. However, it is also important to have reliable ($Mg^{2+}$/$Li^+$)-O-H bond angle parameters to simulate accurately the reorientation of -OH groups. These parameters are not yet available in the ClayFF interaction potential.[60]

The difference of 57% in the amount of $CO_2$ intercalation between our simulations using flexible -OH groups and experimental studies with hectorite[12] are probably related to the lower structural charge (-0.7|*e*| *vs* -1.0|*e*|) and the approximately 55% F for OH substitution in the experimental sample. Consequently, there are more interlayer $Na^+$ ions present in the simulated model, and additional $Na^+$ attracts more $H_2O$ molecules into the interlayer. Both effects lead to a greater interlayer volume occupied by $Na^+$ and $H_2O$ at a given interlayer spacing, and to less interlayer volume available for $CO_2$. This difference is probably offset by the F for OH substitution, which leads to a slightly more hydrophobic surface[74] and a weaker $Na^+$ interaction with it. Thus, the agreement of the simulations with rigid -OH groups and the experiments is probably fortuitous. To validate our hypothesis, interlayer structure and dynamics with flexible and rigid –OH groups are discussed below.

The smaller interlayer $CO_2$ mole fraction for hectorite with flexible -OH groups *vs* earlier studies of Na-montmorillonite is probably related to the differences in the force fields used,[51] the total structural charge and its location, and the orientation of the structural -OH groups.[48-51] The Na-montmorillonite simulations used a lower structural charge (-0.8|*e*|) and rigid –OH groups

oriented parallel to the basal surface. The effects of the differences in force field and -OH group orientation for hectorite and montmorillonite on interlayer structure and dynamics has been recently reported.[31] These results show that the electrostatic repulsion between cations on the octahedral sites and surface $Na^+$ ions are higher in the simulations of Botan et al.[51] compared to those reported here, because the force field parameterization employed by Botan et al.[51] assigned full formal charges to atoms in the octahedral sheet. Makaremi et al.[48] and Rao et al.[49] used ClayFF as in our study, and the larger $CO_2$ mole fractions they found are probably due to the smaller structural charge and to the orientation of the -OH groups. In their studies, the -OH groups were constrained to be oriented parallel to the basal surface, in contrast to our flexible model, in which -OH groups may take parallel or perpendicular orientations depending on whether they are coordinated to substituted or non-substituted octahedral sites, respectively.

The computed immersion energies for Na-hectorite at all *T-P* combinations investigated show global minima at basal spacings of 15.0 Å and 15.4 Å with flexible and rigid -OH groups, respectively (Figures 2a-2d). These results show that the 2WL structure is the stable state under the *T-P* conditions investigated with $H_2O$-saturated *sc*$CO_2$. This conclusion is in good agreement with experimental studies of Na-hectorite and Na-montmorillonite, which show expansion to a 2WL hydrate in contact with $H_2O$-saturated *sc*$CO_2$.[12,14,18,21,43,44] and with swelling free energies reported from MC simulations of Na-montmorillonite, which demonstrate global minima at basal spacings corresponding to 2WL structures (~15.0 Å - 16.0 Å) for $H_2O$ and $CO_2$ intercalation.[48-51] Our results and earlier MC studies agree that the stable 2WL state has a low interlayer mole fraction of $CO_2$.[48-51] In our calculations there are also shallow energy minima at basal spacings of ~12.2 Å at all *T-P* combinations examined indicating metastability of the 1WL state. At basal

spacings greater than that for 2WL, the immersion energies show little variation indicating a low energy cost for further expansion.

**Atomic Density Profiles:**

The atomic density profiles (APDs) of the intercalated $Na^+$, $H_2O$, and $CO_2$ as functions of distance normal to the hectorite basal surface show significant differences in interlayer structure between 1WL and 2WL hydrates with flexible and rigid -OH groups (Figures 3 and 4). Although 2WL is the most thermodynamically stable state, molecular scale understanding of the 1WL state provides insight of the origin of the energetic differences and the transformation between high and low $CO_2$ content. In all cases, the ADPs become broader with increasing *T* and *P* (Figures 3a-3f, 4a-4f and S1, S2), and the broadening is greater for the 1WL structure.

For the 1WL structure with flexible -OH groups, the APD of $Na^+$ shows two peaks of equal intensity at ~2.4 Å and 3.3 Å with significant intensity between them for all *T-P* ranges examined. The two peaks correspond to the same type of adsorption site (above basal surface oxygen atoms, $O_b$) on the two basal surfaces, and the intensity between them indicates that $Na^+$ ions hop between these two sites (Figure 3a-3c). The ADPs of $C_{CO2}$ and $O_{CO2}$ are characterized by single broad peaks located in the midplane of the interlayer with maxima at ~2.8 Å. This distribution indicates that interlayer $CO_2$ molecules are on average oriented with their O-C-O axes parallel to the basal surfaces and undergo limited rocking motion perpendicular to the basal surfaces. The ADP of $O_{H2O}$ consists of a broad peak centered at the interlayer midplane at ~2.8 Å with small shoulders on either side closer to the basal surfaces. Correspondingly, the $H_{H2O}$ APD shows four resolvable features with prominent peaks at ~1.8 Å and 3.9 Å and shoulders near 2.4 Å and 3.3 Å with a very small barrier between them. The ~1.0 Å distance between the $O_{H2O}$

and prominent $H_{H2O}$ peaks indicates that the interlayer $H_2O$ are oriented with one $H_{H2O}$ atom pointed towards the basal surfaces with the other sharing the same plane as the $O_{H2O}$ and participating in H-bonding interactions among $H_2O$ molecules. Previous studies[31,33] have shown that a small number of $H_2O$ in the shoulder region are probably adsorbed at the center of ditrigonal cavities with both $H_{H2O}$ atoms pointing to the basal surface.

The ADPs of each interlayer species in the 1WL structure with rigid -OH groups are generally similar to those with flexible -OH groups, but the peaks and shoulders for the individual environments are broader, and the interlayer midplane is at ~3.0 Å (Figures 4a-4c). The larger intensities for $C_{CO2}$ and $O_{CO2}$ are due to the larger interlayer $CO_2$ contents, as shown in the adsorption isotherms (Figure 1a-1d). Despite having flat tops, the ADPs of $O_{H2O}$ and $H_{H2O}$ indicate a similar structural arrangement to the flexible -OH case. The most important differences in the ADPs between the flexible and rigid -OH models are the distinct shoulders for both $O_{H2O}$ and $H_{H2O}$ at distances closer to the surface ($z$ <2.5 Å) with rigid -OH groups, suggesting that a larger fraction of the $H_2O$ is located above the centers of ditrigonal cavities coordinating to the surface through both their $H_{H2O}$ atoms. The APDs of the $CO_2$ with flexible and rigid -OH groups agree with high pressure NMR studies of hectorite that indicate that on average the interlayer $CO_2$ are oriented parallel to the basal surface at 1WL basal spacings.[12] These results agree well with previous simulation studies using montmorillonite that show the $CO_2$ located at the interlayer midplane and lying parallel to the basal surfaces in 1WL structures under similar conditions.[48-51]

The ADPs of $H_2O$ in the 2WL structures are different than those of the 1WL structures (Figures 3d-3f) and are similar to the 2WL hydrates without $CO_2$ found by Morrow et al.[28] under ambient conditions. The ADPs of $CO_2$ at 2WL basal spacings (15.0 Å) with flexible -OH groups

are not observable because of the small number of interlayer $CO_2$ molecules. A small fraction (~10%) of $Na^+$ are adsorbed at distances ~2.4 Å from the basal surfaces due to the unrestricted motion of the -OH groups. Consequently, there is a significant shoulder for $O_{H2O}$ at distances of < 2.0 Å from the basal surfaces that represents $H_2O$ coordinating the inner-sphere adsorbed $Na^+$ ions. This conclusion is supported by the lack of $Na^+$ ions in this location with rigid -OH groups, where the O-H bond is oriented perpendicular to the basal surface and repulses $Na^+$ ions from the centers of the ditrigonal cavities by the positively charged $H_{OH}$ atoms. With rigid -OH groups, the APD maxima of the $C_{CO2}$ and $O_{CO2}$ atoms are located ~2.9 Å from the basal surfaces (Figures 4d-4f), and $O_{CO2}$ exhibits a shoulder closer to the basal surface at ~2.3 Å. This shoulder indicates a higher probability for $CO_2$ to probe more orientations and to be less dynamically restricted than at 1WL basal spacings, in agreement with recent NMR studies of hectorite under similar physical conditions.[12] Shoulders for $O_{CO2}$ near the basal surfaces indicate that $CO_2$ undergoing a rocking motion, as illustrated by Bowers et al.[12] With both flexible and rigid -OH, $Na^+$ ions are adsorbed as outer sphere complexes, as observed previously by Morrow et al.[28] The intensity difference in the $O_{H2O}$ and $H_{H2O}$ ADPs between flexible and rigid -OH groups is due to the smaller number of interlayer $H_2O$ in the latter case and is similar to previous computational studies for Na-hectorite under ambient conditions.[28] The ADPs of $Na^+$, $H_2O$, and $CO_2$ in the 2WL structure are consistent with simulation studies of montmorillonite with $H_2O$–saturated $CO_2$.[48-51] Although varying pressure from 90 to 150 bar has no significant effect on the ADPs of either the 1WL or 2WL structures (Figures 3, 4 and S1 – S2), increasing temperature from 323 K to 368 K at each modeled pressure causes the peaks to broaden as a result of increased thermal motion, especially for $O_{H2O}$, $H_{H2O,}$ and $Na^+$ with rigid -OH groups.

**$H_2O$ and $CO_2$ Orientation:**

Like the ADPs, the computed mean orientations of intercalated $CO_2$ and $H_2O$ at 1WL and 2WL basal spacings do not vary greatly with pressure and temperature and are generally similar for flexible and rigid -OH groups (Figures 5 and 6). For the 1WL and 2WL hydrate structures, the mean orientation of the O-C-O axis is at 90º with respect to the surface normal for flexible and rigid -OH groups (Figure 5a- 5d). This result indicates that on average the interlayer $CO_2$ molecules lie parallel to the basal surfaces. In both structures, however, the O-C-O axes dynamically occupy a range of angles. For the flexible and rigid -OH groups, the angular distribution is larger for the 2WL hydrate (35º-145º) than for the 1WL hydrate (57º-123º). Both values represent a rocking motion, and the absence of well-separated peaks for the 90º and non-parallel orientations suggests that individual $CO_2$ molecules occur in parallel and non-parallel. The angular distribution of the O-C-O axis in the 1WL is broader with rigid -OH groups (12.5 Å) than with flexible groups (12.2 Å). However, in both, the broad distribution at 1WL basal spacings indicates rocking motion of the $CO_2$ between the two basal surfaces, as proposed by Bowers et al.[12] The absence of O-C-O orientations near 0º and 180º even for the 2WL indicates that $CO_2$ do not undergo isotropic reorientation and does not occur in orientations perpendicular or at high angles to the basal surfaces. As observed in the NMR studies of Bowers et al.,[12] the interlayer $CO_2$ in 2WL show a greater range of computed orientations with respect to the basal surfaces than in 1WL. This distribution produces a narrower but non-zero $^{13}C$ NMR CSA pattern. The computed orientations are in good agreement with $CO_2$ intercalation in montmorillonite under similar *T-P* conditions.[48] The greater peak intensity in the angular distribution for the rigid -OH calculations is a result of the higher interlayer $CO_2$ content with rigid -OH groups.

For the 1WL structure, the mean orientation of the $H_2O$ dipole is 90º with respect to surface normal (parallel to the basal surfaces; Figures 6a-6d) with both rigid and flexible -OH groups. Consequently, the H-H vector has three angular orientations: (i) pointed towards the basal surface (~25º), (ii) parallel to the basal surface (~90º), and (iii) pointed away from the basal surface (160º). The angles at 25º and 160º correspond to the same dipole orientation to one of the surfaces and the 90º value corresponds to $H_2O$ located in the shoulder region of the ADPs (see Figures 3 and 4) and is due to $H_2O$ adsorbed above the center of ditrigonal cavities with both $H_{H2O}$ atoms pointing towards the basal surface. This orientation is abundant with rigid -OH groups, because many $H_2O$ occupy the centers of ditrigonal cavities (Figures 4a-4c). The low- and high-angle values indicate that $H_2O$s are coordinated to the basal surface through one of the $H_{H2O}$ atoms. The larger interlayer $CO_2$ content with rigid -OH groups causes a narrower angular distribution of the $H_2O$ (45º-135º) compared to the lower $CO_2$ content with flexible -OH groups (30º-150º; Figure 6a and 6b). This difference is due to different computational parameters, but increasing $CO_2$ content probably causes a reduced range of motion for the $H_2O$ in general.

For the 2WL structure, the $H_2O$ dipole and H-H vectors explore nearly similar angular distributions, with dominant peaks at 90º and broader peaks at 47º and 133º with flexible and rigid -OH groups (Figure 6c and 6d). This result indicates that the $H_2O$ molecules are oriented as in the 1WL case but exhibit a wider range of possible orientations. The difference in $H_2O$ content between rigid and flexible -OH groups causes differences in intensity of the angular distribution profiles. This is in good agreement with previous MD simulations under ambient conditions with only interlayer $H_2O$ and with Na-montmorillonite using an external $H_2O$ saturated $CO_2$ rich fluid phase.[28,51]

**Planar Atomic Density Distributions**

Planar atomic density distributions (PADDs) provide a more comprehensive depiction of $O_b$ and $Na^+$ relations to the time-averaged structural environments of intercalated $H_2O$ and $CO_2$.[31,33] The PADDs in Figures 7a-7d show significant variations between the 1WL and 2WL with flexible and rigid -OH groups at 323 K and 90 bar.

The PADDs of the $Na^+$ and $CO_2$ for the 1WL (12.2 Å - flexible and 12.5 Å - rigid) show that both models have $Na^+$ located at 2.4 Å and 3.3 Å in the ADPs (see Figures 3a and 4a) with sites above the $O_b$ of both basal surfaces and that the $Na^+$ ions hop between the two basal surfaces (Figures 7a and 7b), in agreement with the atomic density profiles (Figure 3). In contrast, the adsorption sites of $CO_2$ differ depending on the -OH model. With flexible -OH groups, the $CO_2$ is located with one $O_{CO2}$ directly above an $O_b$ of one surface and the other above the center of a ditrigonal cavity on the opposing basal surface (Figure 7a). With rigid -OH groups, one $O_{CO2}$ is located at the center of a ditrigonal cavity on both basal surfaces and the other $O_{CO2}$ is located on average directly above the trigonal plane of Si tetrahedra on both basal surfaces (Figure 7b). The two tetrahedral sheets adjacent to the interlayer superpose in projection for the rigid -OH simulations, whereas they are offset significantly with flexible -OH groups. This difference indicates that lateral displacement of the T-O-T layers are significantly correlated with the orientation of the structural -OH groups and interlayer distances (12.2 Å *vs* 12.5 Å), thus resulting in different adsorption structures for $CO_2$ in the 1WL structure. Because the -OH groups are oriented perpendicular to the basal surface with the rigid model, the smectite layer becomes more hydrophobic compared to the flexible model, thus making $Na^+$ less strongly adsorbed by the surface. This interpretation is in good agreement with the more diffuse lateral distribution of $Na^+$ with rigid -OH groups (Figure 7b) compared to flexible -OH groups (Figure 7a). Consequently, adsorption of $CO_2$ and displacement of T-O-T layers with flexible -OH

groups are in reasonable agreement with Botan et al.[51] for montmorillonite, where the -OH groups were oriented parallel to the basal surface. Although $CO_2$ adsorption here is similar to that determined by Botan et al.[51] the displacement of the T-O-T layers is different. Aggregation of $CO_2$ is more evident with rigid -OH groups, probably due to the higher interlayer $CO_2$ mole fraction. In these $CO_2$ clusters, the molecules mostly have a slipped parallel arrangement (parallel $CO_2$ with slight offset) with respect to each other, as reported by Sena et al.[52] for Na-montmorillonite. This geometry is favorable for small clusters of $CO_2$ in montmorillonite.[52] T-shaped orientated $CO_2$ clusters is not observed here.

The PADDs for $H_2O$ at 1WL spacings also show significant differences with flexible and rigid -OH groups (Figures 7c and 7d). The $H_2O$ in the shoulder regions of the ADPs at distances < 2.3Å from a basal surface (Figures 3 and 4) are located above the centers of ditrigonal cavities with both $H_{H2O}$ atoms coordinating to $O_b$, as discussed above based on the ADPs and molecular orientations. This fraction of $H_2O$ is higher with rigid -OH groups than with flexible -OH, due to the larger basal spacing (12.5 Å *vs* 12.2 Å, respectively). Consequently, the contours of $H_{H2O}$ are more strongly localized around $O_{H2O}$ at the center of ditrigonal cavities with flexible -OH groups than with rigid -OH. The $H_2O$ represented by the dominant peak at ~2.8 Å in the ADPs coordinate with $O_b$ through one of the $H_{H2O}$ with flexible and rigid –OH groups (Figure 7e and 7f). The contours of the $O_{H2O}$ and $H_{H2O}$ show a more dispersed pattern with rigid -OH groups than with flexible -OH. More $CO_2$ leads to the formation of small $CO_2$ clusters, in addition to showing stronger coordination with the basal surface in the rigid -OH model. These small $CO_2$ clusters show strong coordination with the basal surface while $H_2O$ interactions with surface $O_b$ atoms is restricted to the immediate neighborhood of the $Na^+$. This result is in excellent agreement with the $H_2O$ angular distributions (Figures 6b), which show slightly more restricted

angular dynamics with rigid -OH groups, and with the PADDs of previous studies of hydrated Na-hectorite.[32]

For the 2WL structures, the PADDs of $Na^+$ ions show poorly defined contours regardless of the -OH type (Figures 8a and S3), consistent with $Na^+$ in outer sphere coordination exhibiting greater lateral diffusion than those in inner sphere coordination in the 1WL complexes. The small fraction of $Na^+$ ions located at distances < 2.5 Å from the basal surfaces with flexible -OH groups are located above $O_b$ atoms and are more dynamically restricted than those at the interlayer midplane. On average, the adsorption pattern of $CO_2$ in the 2WL structures with rigid -OH groups are not greatly different from those with 1WL with rigid -OH groups (Figure 8b). One $O_{CO2}$ is located above a silicon tetrahedron and the other is located above the center of a ditrigonal cavity. Neither $O_{CO2}$ is, however, well localized at its adsorption site. In accord with the ADP results that show the $CO_2$ located near one basal surface and not at the midplane of the interlayer, this result indicates that, unlike in 1WL structure, the $CO_2$ adsorbed on one surface is not affected by the other basal surface. This conclusion is consistent with the experimental NMR results of Bowers et al.[12] and the computed $CO_2$ angular distribution in this study (Figure 5d).

The PADDs of the $H_2O$ for 2WL with flexible and rigid -OH groups are similar to previous studies of hydrated Na-hectorite,[28] and are not discussed further. However, the PADDs for $H_2O$ in the shoulder region at distances $z$ < 2.5 Å with flexible -OH groups confirm that these $H_2O$ are adsorbed above the centers of ditrigonal cavities with both $H_{H2O}$ atoms coordinated to the surface, consistent with our H-bonding profiles (See Supporting Information, Figure S4 and S5). The PADDs of $Na^+$, $CO_2$ and $H_2O$ exhibit more disordered contours with increasing $T$ and $P$, but the overall interlayer structure does not change significantly.

The experimental $^{13}CO_2$ NMR results for hectorites at 50°C and 90 bar show a uniaxial $^{13}C$ spinning sideband pattern due to chemical shift anisotropy (CSA) of dynamically restricted $CO_2$.[12] The results show that on average the $CO_2$ molecules lie with their O-C-O axes parallel to the basal surfaces, in agreement with the computed results here for 1WL and 2WL structures. The NMR results also show that the $CO_2$ molecules undergo rapid rotation or libration around an axis perpendicular to their O-C-O axes at frequencies of at least ~$10^5$ Hz. In the simulations here, the PADDs for $O_{CO2}$ and $C_{CO2}$ do not clearly show complete isotropic averaging of the $CO_2$ orientations in the *x*-*y* plane over the 5 ns time scale represented in these diagrams, especially at 1WL basal spacings with flexible -OH groups. These results suggest that the characteristic frequency of rotation or libration of interlayer $CO_2$ are between ~$10^5$ Hz and ~$10^8$ Hz.

**Residence Times:**

The computed residence times for nearest neighbor coordination among pairs of species and surface $O_b$ show less dynamical stability for interactions involving $CO_2$ than $H_2O$ and shorter residence times for 2WL than 1WL and with increasing temperature (Table 3). Pressure in the range examined has little effect on residence times, and only values for $P$ = 120 and 150 bar are shown in Tables S1 and S2. Importantly, the use of the flexible and rigid -OH models has little effect on the calculated residence times (Table 3). As expected, the intermittent residence times $c(t)$ are much longer than the continuous times $C(t)$,[31,33,73] demonstrating that individual atomic pairs often re-coordinate after separation. Regardless of the -OH model, $Na^+$ ions spend much longer in NN coordination with $H_2O$ than with $CO_2$ at both 1WL and 2WL. This result is consistent with $Na^+$ preference to coordinate with $H_2O$ than with $CO_2$ due to their larger solvation energy with $H_2O$ (~410 kJ/mol *vs* ~293 kJ/mol).[75,76] The residence times of $CO_2$ associated with $H_2O$ and $O_b$ are substantially longer than with $Na^+$ at both the 1WL and 2WL

states, resulting in $CO_2$ being adsorbed closer to the basal surfaces surrounded by $H_2O$. Because of the low $CO_2$ mole fraction in the 2WL structure with flexible -OH groups, the residence times were smaller than the time interval (2 ps) used to compute these values, and are not reported in Tables 3, S1 and S2.

For the 1WL state with flexible and rigid -OH groups, the residence times of $Na^+$ in coordination with $H_2O$ and $O_b$ are similar to each other, as expected for the strongly hydrated $Na^+$. However, the residence times for $H_2O$-$O_b$ and $Na^+$-$H_2O$ pairs are ~50% lower in the 2WL structure than for the same pairs in the 1WL structure. This difference indicates rapid dynamical exchange of $H_2O$ between these sites in NN coordination to $Na^+$ and $O_b$ outside their current coordination shells, in good agreement with the PADD and RDF results (see Supporting Information, Figures S6 and S7). Because $Na^+$ ions are adsorbed exclusively as outer sphere surface complexes in the 2WL structure with rigid -OH groups, no lifetimes for $Na^+$ - $O_b$ pairs are reported.

## Conclusions

Computational molecular modeling of $CO_2$ and $H_2O$ intercalation in the interlayers of a smectite clay (Na-hectorite) in equilibrium with $H_2O$-saturated $CO_2$ at temperatures and pressures relevant to the subsurface conditions of enhanced oil recovery, shale gas exploration, and geologic carbon sequestration provide detailed insight into the partitioning of $CO_2$ and $H_2O$ between clay interlayers and pore fluids, the energetics of these interactions, and the structural and dynamical behavior of the interlayer species and their interaction with the clay substrate. The simulations use a Grand Canonical Molecular Dynamics (GCMD) technique that allows the clay layers to move laterally with respect to each other, which is essential for obtaining the correct

interlayer structure and system energy. This is the first time that this technique has been used for layer structure materials or for fluid reservoirs containing two components. Compared to the more commonly used approach of Grand Canonical Monte Carlo (GCMC) calculations followed by separate classical Molecular Dynamics (MD) calculations, GCMD has the advantages of computing adsorption isotherms and related structural and dynamical properties simultaneously using the same simulation trajectories.

The general features of the results for $CO_2$ and $H_2O$ partitioning between the external fluid and the interlayer agree reasonably well with previous simulations of the comparable Na-montmorillonite smectite using GCMC methods and with experimental results for hectorite and montmorillonite.[12,14,16,18,19,22,43-51] The calculated immersion energies as functions of basal spacing clearly indicate that 2WL is the stable equilibrium state for Na-hectorite in equilibrium with $H_2O$-saturated $CO_2$ at $T$ between 323 K and 368 K and $P$ between 90 and 150 bars, consistent with experimental observations.[12] The computed basal spacing of fully collapsed Na-hectorite with no interlayer $CO_2$ or $H_2O$ is 9.5 Å, but significant intercalation of $CO_2$ begins at ~11.2 Å, where the interlayers are propped open by $H_2O$ in amounts less than required to form a complete monolayer (<1WL). This conclusion is in good agreement with previous experimental studies of Na-montmorillonite and Na-hectorite.[12,14,16,18,19,22,43-46] The computed $CO_2$ content increases with increasing basal spacing and reaches a maximum for the 1WL state with basal spacings of ~12.2 Å ("flexible" model) and 12.5 Å ("rigid" model) and then decreases with increasing basal spacing, in agreement with previous experimental and simulation studies.[12,43,44,48-51]

The simulations show that for the 1WL state $CO_2$ molecules are located at the midplane of the interlayer with rocking motion between two basal surfaces, whereas for the 2WL state they

are located closer to one or the other basal surface (at ~2.8 Å). For 1WL and 2WL hydration states, the $CO_2$ have a mean orientation with their O-C-O axis parallel to the basal surfaces. The broad range of angular distribution for $CO_2$ in the 2WL state indicates that these molecules are less restricted when compared to the 1WL state, consistent with experimental results by Bowers et al.[12] Our studies indicate that the range of rotational motion for the $H_2O$ decreases with increasing $CO_2$ content for the rigid -OH model where the -OH group is held rigidly perpendicular to the clay layers during simulation.

With the flexible -OH model, in which the structural -OH orientation is allowed to vary, $CO_2$ are adsorbed with one $O_{CO2}$ above a surface oxygen ($O_b$) from each basal surface with the other $O_{CO2}$ at the center of a ditrigonal cavity for the 1WL state. Importantly, the $O_{CO2}$ that are located near $O_b$ on one basal surface are located at the center of ditrigonal cavities of the opposite basal surface. In contrast, with the rigid -OH model, one $O_{CO2}$ is located at the center of a ditrigonal cavity and the other $O_{CO2}$ is above a Si tetrahedron of each basal surface. The local adsorption environment varies with the same $O_{CO2}$ atoms sharing Si tetrahedron from both basal surfaces, unlike with the flexible model for the 1WL state. This difference in local adsorption environment is accomplished by the lateral re-arrangement of clay TOT layers with respect to each other between flexible and rigid -OH models. The $CO_2$ adsorption structure in the 1WL state using the flexible model is in good agreement with simulations of Botan et al.[51] for montmorillonite. The difference in the $CO_2$ local adsorption structure with the 1WL "rigid" model is likely due to the fixed perpendicular orientation of the -OH groups to the surface and related changes in the lateral arrangement of the TOT layers. However, the local adsorption environment of intercalated $CO_2$ in the 2WL state is not greatly different from the 1WL state with one $O_{CO2}$ atoms near Si tetrahedra and the other at the ditrigonal cavity centers with rigid -

OH groups. The poorly defined time-averaged surface atomic density contours for $O_{CO2}$ and $C_{CO2}$ combined with the greater range of rotational mobility of $CO_2$ clearly indicate that the interlayer structure is not impacted by an opposing basal surface in the 2WL hydration state, which is consistent with Botan et al.[51] studies on montmorillonite under similar conditions.

The interlayer $CO_2$ aggregate into small clusters (mostly as dimers) and are always in a slipped parallel geometric arrangement with rigid -OH model, as found in earlier MD simulations.[52] The formation of small $CO_2$ clusters is considerably reduced in the model with flexible -OH groups because of the lower interlayer mole fraction of $CO_2$. The interlayer $H_2O$ are predominantly adsorbed in a structural arrangement with one $H_{H2O}$ coordinating with surface $O_b$ and the other $H_{H2O}$ coordinating with other $H_2O$ as illustrated by Morrow et al.[28] with pure $H_2O$ simulations. However, we observe a significant fraction of $H_2O$ located at the center of the ditrigonal cavities with both $H_{H2O}$ coordinating to the basal surface for each -OH models at 1WL distances with high $CO_2$ adsorption in contrast to previous simulations on Na-hectorite.[28] This $H_2O$ fraction is more prominent in the 2WL structure, especially with the flexible -OH model. This difference indicates that, in addition to the interlayer $CO_2$ content, the motion of the structural -OH groups plays an important role in defining the local coordination environment of the interlayer $H_2O$ molecules. The interlayer structure does not vary significantly in the *T-P* ranges examined in this study (from 323 to 368 K and from 90 to 150 bar, respectively), but the dynamics of the systems becomes more rapid with increasing temperature, as expected. For instance, the site residence times for all neighboring atomic pairs decrease with increasing temperature due to increased thermal motion. The residence times of different atomic pairs in the interlayer corroborate the RDF calculations that the coordination of $CO_2$ and $Na^+$ is unlikely, as observed for Na-montmorillonite in contact with water-saturated $CO_2$ fluid[49,51] (see Supporting

Information). Instead, $CO_2$ molecules are preferably coordinated with surface atoms and $H_2O$ at 1WL and 2WL basal spacings and with both rigid and flexible -OH models.

The modeled flexibility of the structural -OH groups coordinated to the octahedral sites of the T-O-T layers and located at the base of the ditrigonal cavities affects the calculated interlayer $CO_2$ mole fraction, basal spacing, and structure, but the overall behavior and trends of these values with basal spacing are similar. Despite identical structural charge, the hectorite model with flexible -OH groups have a lower interlayer $CO_2$ content at all basal spacings than the model with -OH groups rigidly fixed perpendicular to the basal surfaces. With flexible -OH groups, the equilibrium 2WL structure contains few $CO_2$ molecules. The computed $CO_2$ mole fractions using the rigid -OH model is closer to experimental values than with the flexible -OH model.[12] This agreement may arise from the difference of $F^-$ for $OH^-$ substitution in the experimental sample together with the layer charge difference of -0.2|*e*| when compared to the simulated model. Any discrepancies with montmorillonite calculations can be attributed to the imposed orientation of the structural -OH groups in montmorillonite parallel to the basal surfaces, in contrast to the imposed perpendicular orientation with our rigid -OH model, and to the structural charge differences.[48-51] For future studies with hectorite, a reliable ($Mg^{2+}$/$Li^+$)-OH bond angle potential should be developed to realistically model the motion of the -OH groups, following the approach recently developed for brucite and gibbsite.[77] Our studies also indicate that even small differences in structural layer charge, orientation of the structural -OH groups, and the composition of the octahedral sheet can critically affect the interlayer adsorption, structure and dynamics of the intercalated species in smectites.

## ACKNOWLEDGMENTS

All the calculations were performed using computational resources at the National Energy Research Scientific Computing Center, which is supported by the Office of Science of the U.S. Department of Energy under ECARP No. m1649. The authors acknowledge the iCER computational facility at Michigan State University for additional computational resources. The work described in this paper was supported by the United States Department of Energy, Office of Science, Office of Basic Energy Science, Chemical Science, Biosciences, and Geosciences division through the sister grants DE-FG02-10ER16128 (Bowers, P.I.) and DE-FG02-08ER15929 (Kirkpatrick, P.I., Yazaydin, co-PI). A.G.K. acknowledges the support of the industrial chair "Storage and Disposal of Radioactive Waste" at the Institut Mines-Télécom Atlantique, funded by ANDRA, Areva, and EDF.

**Notes**

The authors declare no competing financial interest.

## References


1. Holloway, S. Storage of Fossil Fuel-Derived Carbon Dioxide Beneath the Surface of the Earth. *Ann. Rev. Energy. Environ.* **2001**, *26*, 145-166.
2. Lackner, K. S. A Guide to $CO_2$ Sequestration. *Science* **2003,** *300*, 1677-1678.
3. Benson, S. M.; Cole, D. R. $CO_2$ Sequestration in Deep Sedimentary Formations. *Elements* **2008,** 4, 325-331.
4. Bachu, S.; Bonijoly, D.; Bradshaw, J.; Burruss, R.; Holloway, S.; Christensen, N. P.; Mathiassen, O. M. $CO_2$ Storage Capacity Estimation: Methodology and Gaps. *Int. J. Green. Gas Cont.* **2007,** 1, 430-443.
5. Wilkin, R. T.; Digiulio, D. Geochemical Impacts to Groundwater from Geologic Carbon Sequestration: Controls on pH and Inorganic Carbon Concentrations from Reaction Path and Kinetic Modeling. *Environ. Sci. Technol.* **2010,** 44, 4821-4827.
6. Ochs, M.; Boonekamp, M.; Wanner, H.; Sato, H.; Yui, M. A Quantitative Model for Ion Diffusion in Compacted Bentonite. *Radiochim. Acta* **1998**, *82*, 437-444.
7. Weiss, C. A.; Kirkpatrick, R. J.; Altaner, S. P. Variations in Interlayer Cation Sites of Clay Minerals as Studied by $^{133}Cs$ MAS Nuclear Magnetic Resonance Spectroscopy. *Amer. Mineral.* **1990**, *75*, 970-982.
8. Altmann, S.; Tournassat, C.; Goutelard, F.; Parneix, J. C.; Gimmi, T.; Maes, N. Diffusion-Driven Transport in Clayrock Formations. *Appl. Geochem.* **2012**, *27*,463-478.
9. Meakin, P.; Tartakovsky, A. M. Modeling and Simulation of Pore-Scale Multiphase Fluid Flow and Reactive Transport in Fractured and Porous Media. *Rev. Geophys.* **2009**, 47, RG3002.
10. Davis, A. J.; Kent, B. D. Surface Complexation Modeling in Aqueous Geochemistry. *Rev. Mineral.* **1990**, *23*, 177-260.
11. Bowers, G. M.; Hoyt, D. W.; Burton, S. D.; Ferguson, B. O.; Varga, R.; Kirkpatrick, R. J. In Situ $^{13}C$ and $^{23}Na$ Magic Angle Spinning NMR Investigation of Supercritical $CO_2$ Incorporation in Smectite-Natural Organic Matter Composites. *J. Phys. Chem. C* **2014,** *118*, 3564-3573.
12. Bowers, G. M.; Schaef, H. T.; Loring, J. S.; Hoyt, D. W.; Burton, S. D.; Walter, E. D.; Kirkpatrick, R. J. Role of Cations in $CO_2$ Adsorption, Dynamics and Hydration in Smectite Clays under In Situ Supercritical $CO_2$ Conditions. *J. Phys. Chem. C* **2017,** *121*, 577-592.
13. Wang, Z.; Felmy, A. R.; Thompson, C. J.; Loring, J. S.; Joly, A. G.; Rosso, K. M.; Schaef, H. T.; Dixon, D. A. Near-Infrared Spectroscopic Investigation of Water in Supercritical $CO_2$ and the effect of $CaCl_2$. *Fluid Phase Equil.* **2013,** *338*, 155-163.
14. Giesting, P.; Guggenheim, S.; van Groos, A. F. K.; Busch, A. Interaction of Carbon Dioxide with Na-Exchanged Montmorillonite at Pressures to 640 bar: Implications for $CO_2$ Sequestration. *Int. J. Green. Gas Cont.* **2012,** 8, 73-81.

15. Lee, M.-S.; McGrail, B. P.; Glezakou, V.-A. Microstructural Response of Variably Hydrated Ca-rich Montmorillonite to Supercritical $CO_2$. *Environ. Sci. Technol.* **2014,** 48, 8612-8619.

16. Ilton, E. S.; Schaef, H. T.; Qafoku, O.; Rosso, K. M.; Felmy, A. R. In Situ X-ray Diffraction Study of $Na^+$ Saturated Montmorillonite Exposed to Variably Wet Supercritical $CO_2$. *Environ. Sci. Technol.* **2012,** 46, 4241-4248.

17. Giesting, P.; Guggenheim, S.; van Groos, A. F. K.; Busch, A. X-ray Diffraction Study of K- and Ca-Exchanged Montmorillonites in $CO_2$ Atmospheres. *Environ. Sci. Technol.* **2012,** 46, 5623-5630.

18. Guggenheim, S.; van Groos, A. F. K. An Integrated Experimental System for Solid-Gas-Liquid Environmental Cells. *Clays Clay Miner.* **2014,** 62, 470-476.

19. Rother, G.; Ilton, E. S.; Wallacher, D.; Hauss, T.; Schaef, H. T.; Qafoku, O.; Rosso, K. M.; Felmy, A. R.; Krukowski, E. G.; Stack, A. G.; et al. $CO_2$ Sorption to Subsingle Hydration Layer Montmorillonite Clay Studies by Excess Sorption and Neutron Diffraction Measurements. *Environ. Sci. Technol.* **2013,** 47, 205-211.

20. Schaef, H. T.; Ilton, E. S.; Qafoku, O.; Martin, P. F.; Felmy, A. R.; Rosso, K. M. In Situ X-RD study of $Ca^{2+}$ Saturated Montmorillonite (STx-1) Exposed to Anhydrous and Wet Supercritical Carbon Dioxide. *Int. J. Green. Gas Cont.* **2012,** 6, 220-229.

21. Romanov, V. N. Evidence of Irreversible $CO_2$ Intercalation in Montmorillonite. *Int. J. Green. Gas Cont.* **2013,** 14, 220-226.

22. Schaef, H. T.; Loring, J. S.; Glezakou, V. A.; Miller, Q. R. S.; Chen, J.; Owen, A. T.; Lee, M.-S.; Ilton, E. S.; Felmy, A. R.; McGrail, B. P.; Thompson, C. J. Competitive Sorption of $CO_2$ and $H_2O$ in 2:1 Layer Phyllosilicates. *Geochim. Cosmochim. Acta* **2015,** 161, 248-257.

23. Bowers, G. M.; Bish, D. L.; Kirkpatrick, R. J. Cation Exchange at the Mineral-Water Interface: $H_3O^+/K^+$ Competition at the Surface of Nano-Muscovite. *Langmuir* **2008**, *24*, 10240-10244.

24. Teich-McGoldrick, S. L.; Greathouse, J. A., Cygan, R. T. Molecular Dynamics Simulations of Uranyl Adsorption and Structure on the Basal Surface of Muscovite. *Molec. Simul.* **2014**, *40*, 610-617.

25. Bowers, G. M.; Singer, J. W.; Bish, D. L.; Kirkpatrick, R. J. Alkali Metal and $H_2O$ Dynamics at the Clay/Water Interface. *J. Phys. Chem. C* **2011**, *115*, 23395-23407.

26. Marry, V.; Dubois, E.; Malikova, N.; Durand-Vidal, S.; Longeville, S.; Breu, J. Water Dynamics in Hectorite Clays: Influence of Temperature Studied by Coupling Neutron Spin Echo and Molecular Dynamics. *Environ. Sci. Technol.* **2011**, *45*, 2850-2855.

27. Weiss, C. A.; Kirkpatrick, R. J.; Altaner, S. P. The Structural Environments of Cations Adsobed onto Clays – $^{133}Cs$ Variable-Temperature MAS NMR Spectroscopic Study of Hectorite. *Geochim. Cosmochim. Acta* **1990**, *54*, 1655-1669.

28. Morrow, C. P.; Yazaydin, A. O.; Krishnan, M.; Bowers, G. M.; Kalinichev, A. G.; Kirkpatrick. R. J. Structure, Energetics and Dynamics of Smectite Clay Interlayer Hydration: Molecular Dynamics and Metadynamics Investigation of Na-Hectorite. *J. Phys. Chem. C* **2013**, *117*, 5172-5187.

29. Reddy, U. V.; Bowers, G. M.; Loganathan, N.; Bowden, M.; Yazaydin, A. O.; Kirkpatrick, R. J. Water Structure and Dynamics in Smectites: $^{2}H$ NMR Spectroscopy of Mg, Ca, Sr, Cs and Pb-Hectorite. *J. Phys. Chem. C* **2016,** *120*, 8863-8876.

30. Marry, V.; Malikova, N.; Cadene, A.; Dubois, E.; Durand-Vidal, S.; Turq, P.; Breu, J.; Longeville, S.; Zanotti, J. M. Water Diffusion in a Synthetic Hectorite by Neutron Scattering – Beyond the Isotropic Translational Model. *J. Phys.: Cond. Matter* **2008**, *20*, 104205.

31. Loganathan, N.; Yazaydin, A. O.; Bowers, G. M.; Kalinichev, A. G.; Kirkpatrick, R. J. Structure, Energetics and Dynamics of $Cs^{+}$ and $H_2O$ in Hectorite: Molecular Dynamics Simulations with Unconstrained Substrate Surface. *J. Phys. Chem. C* **2016**, 1*20*, 10298-10310.

32. Porion, P.; Faugere, A. M.; Delville, A. Multiscale Water Dynamics within Dense Clay Sediments Probed by $^{2}H$ Multiquantum NMR Relaxometry and Two-Time Stimulated Echo NMR Spectroscopy. *J. Phys. Chem. C* **2013**, *117*, 26119-26134.

33. Loganathan, N.; Yazaydin, A. O.; Bowers, G. M.; Kalinichev, A. G.; Kirkpatrick, R. J. Cation and Water Structure, Dynamics and Energetics in Smectite Clays: A Molecular Dynamics Study of Ca-Hectorite *J. Phys. Chem. C* **2016**, *120*, 12429-12439.

34. Greathouse, J. A.; Hart, D. B.; Bowers, G. M.; Kirkpatrick, R. J.; Cygan, R. T. Molecular Simulation of Structure and Diffusion at Smectite-Water Interfaces: Using Expanded Clay Interlayers as Model Nanopores. *J. Phys. Chem. C* **2015**, *119*, 17126-17136.

35. Sobolev, O.; Le Forestier, L.; Gonzalez, M. A.; Russina, M.; Kemner, E.; Cuello, G. J.; Charlet, L. Hydration of $Na^{+,}$ $Ni^{2+}$ and $Sm^{3+}$ in the Interlayer of Hectorite: A Quasi Neutron Scattering Study. *J. Phys. Chem. C* **2009**, *113*, 13801-13812.

36. Bowers, G. M.; Singer, J. W.; Bish, D. L.; Kirkpatrick, R. J. Structure and Dynamical Relationships of $Ca^{2+}$ and $H_2O$ in Smectite/$^{2}H_2O$ Sytems. *Amer. Mineral*. 2014, *99*, 318-331.

37. Ngouana-Wakou, B. F.; Kalinichev, A.G. Structural Arrangements of Isomorphic Substitutions in Smectites: Molecular Simulation of the Swelling Properties, Interlayer Structure and Dynamics of Hydrated Cs-Montmorillonite Revisited with New Clay Models. *J. Phys. Chem. C* **2014**, *118*, 12758-12773.

38. Sato, T.; Watanabe, T.; Otuka, R. Effects of Layer Charge, Charge Location, and Energy Change on Expansion Properties of Dioctahedral Smectites. *Clays Clay Miner.* **1992**, *29*, 873-882.

39. Wang, J.; Kalinichev, A. G.; Kirkpatrick, R. J. Effects of Substrate Structure and Composition on the Structure, Dynamics and Energetics of Water at Mineral Surfaces: A Molecular Dynamics Modeling Study. *Geochim. Cosmochim. Acta* **2006,** *70*, 562-582.

40. Young, D. A.; Smith, D. E. Simulations of Clay Mineral Swelling and Hydration: Dependence upon Interlayer Ion Size and Charge. *J. Phys. Chem. B* **2000**, *104*, 9163-9170.

41. Marry, V.; Turq, P.; Cartailler, T.; Levesque, D. J. Microscopic Simulation of Structure and Dynamics of Water and Counterions in a Monohydrated Montmorillonite. *J. Chem. Phys*. **2002**, *117*, 12769-12775.

42. Smith, D. E. Molecular Computer Simulations of the Swelling Properties and Interlayer Structure of Cesium Montmorillonite. *Langmuir* **1998**, *14*, 5959-5967.

43. Loring, J. S.; Schaef, H. T.; Turcu, R. V. F.; Thompson, C. J.; Miller, Q. R.; Martin, P. F.; Hu, J.; Hoyt, D. W.; Qafoku, O.; Ilton, E. S.; et al. In Situ Molecular Spectroscopic Evidence for $CO_2$ Intercalation into Montmorillonite in Supercritical Carbon Dioxide. *Langmuir* **2012,** *28*, 7125-7128.

44. Loring, J.S.; Ilton, E.S.; Chen, J.; Thompson, C.J.; Martin, P.F.; Benezeth, P.; Rosso, K.M.; Felmy, A.R.; Schaef, H.T. In Situ Study of $CO_2$ and $H_2O$ Partitioning Between Na-Montmorillonite and Variably Wet Supercritical Carbon Dioxide. *Langmuir* **2014,** *30*, 6120-6128.

45. Krukowski, E.G.; Goodman, A.; Rother, G.; Ilton, E.S.; Guthrie, G.; Bodnar, R.J. FT-IR Study of $CO_2$ Interaction with $Na^+$ Exchanged Montmorillonite. *Appl. Clay Sci.* **2015,** *114*, 61-68.

46. Loring, J. S.; Schaef, H. T.; Thompson, C. J.; Turcu, R. V. F.; Miller, Q. R.; Chen, J.; Hu, J.; Hoyt, D. W.; Martin, P. F.; Ilton, E. S.; et al. Clay Hydration/Dehydration in Dry to Water-Saturated Supercritical $CO_2$: Implications for Caprock Integrity. *Energy Procedia* **2013,** *37*, 5443-5448.

47. Myshakin, E. M.; Saidi, W. A.; Romanov, V. N.; Cygan, R. T.; Jordan, K. D. Molecular Dynamics Simulations of Carbon Dioxide Intercalation in Hydrated Na-Montmorillonite. *J. Phys. Chem. C* **2013**, *117*, 11028-11039.

48. Makaremi, M.; Jordan, K. D.; Guthrie, G. D.; Myshakin, E. M. Multiphase Monte Carlo and Molecular Dynamics Simulations of Water and $CO_2$ Intercalation in Montmorillonite and Beidellite. *J. Phys. Chem. C* **2015**, *119*, 15112-15124.

49. Rao, A.; Leng, Y., Molecular Understanding of $CO_2$ and $H_2O$ in a Montmorillonite Clay Interlayer Under $CO_2$ Geological Sequestration Conditions. *J. Phys. Chem. C* **2016**, *120*, 2642-2654.

50. Rao, A.; Leng, Y. Effect of Layer Charge on $CO_2$ and $H_2O$ Intercalations in Swelling Clays. *Langmuir* **2016**, *32*, 11366-11374.

51. Botan, A.; Rotenberg, R.; Marry, V.; Turq, P.; Noetinger, B. Carbon Dioxide in Montmorillonite Clay Hydrates: Thermodynamics, Structure and Transport from Molecular Simulation. *J. Phys. Chem. C* **2010**, *114*, 14962-14969.

52. Sena, M. M.; Morrow, C. P.; Kirkpatrick, R. J.; Krishnan, M. Structure, Energetics, and Dynamics of Supercritical Carbon Dioxide at Smectite Mineral-Water Interfaces: Molecular Dynamics Modeling and Adaptive Force Investigation of $CO_2/H_2O$ Mixtures Confined in Na-Montmorillonite. *Chem. Mater.* **2015**, *27*, 6946-6959.

53. Yazaydin, A. O.; Bowers, G. M.; Kirkpatrick, R. J. Molecular Dynamics Modeling of Carbon Dioxide, Water and Natural Organic Matter in Na-Hectorite. *Phys. Chem. - Chem. Phys.* **2015**, *17*, 23356-23367.

54. Shroll, R.; Smith, D. E. Molecular Dynamics Simulations in the Grand Canonical Ensemble: Application to Clay Mineral Swelling. *J. Chem. Phys.* **1999**, *111*, 9025-9033.

55. Breu, J.; Seidl, W.; Stoll, A., Disorder in Smectites in Dependence of the Interlayer Cation. *Z. Anorg. Allg. Chem*. **2003**, *629*, 503-515.

56. Tenorio, R. P.; Alme, L. R.; Engelsberg, M.; Fossum, J. O.; Hallwass, F. Geometry and Dynamics of Intercalated Water in Na-Fluorohectorite Clay Hydrates. *J. Phys. Chem. C* **2008**, *112*, 575-580.

57. Lowenstein, W. The Distribution of Aluminium in the Tetrahedra of Silicates and Aluminates. *Am. Mineral*. **1954**, *39*, 92-96.

58. Boinepalli, S.; Attard, P. Grand Canonical Molecular Dynamics. *J. Chem. Phys*. **2003**, *119*, 12769-12775.

59. Dubbeldam, D.; Calero, S.; Ellis, D. E.; Snurr, R. Q. RASPA: Molecular Simulation Software for Adsorption and Diffusion in Flexible Nanoporous Materials. *Mol. Simul.* **2016**, *42*, 81-101.

60. Cygan, R. T.; Liang, J.-J.; Kalinichev, A. G. Molecular Models of Hydroxide, Oxyhydroxide and Clay Phases and the Development of a General Force Field. *J. Phys. Chem. B* **2004,** *108*, 1255-1266.

61. Berendsen, H. J. C.; Postma, J. P. M.; Gunsteren, W. F.; van Hermans, J. Interaction Models for Water in Relation to Protein Hydration. In *Intermolecular Forces*; The Jerusalem Symposia on Quantum Chemistry and Biochemistry; Pullman, B., Ed.; Springer: Netherlands, 1981; pp 331−342.

62. Cygan, R. T.; Romanov, V. N.; Myshakin, E. M. Molecular Simulation of Carbon Dioxide Capture by Montmorillonite Using an Accurate and Flexible Force Field. *J. Phys. Chem. C* **2012,** *116*, 13079-13091.

63. Allen, M. P.; Tildesley, D. J. Computer Simulations of Liquids; Clarendon Press: Oxford, U.K., 1987.

64. Shinoda, W.; Shiga, M.; Mikami, M. Rapid Estimation of Elastic Constants by Molecular Dynamics Simulations under Constant Stress. *Phys. Rev. B.* **2004,** *69*, 134103.

65. Spycher, N.; Pruess, K.; Ennis-King J. $CO_2$-$H_2O$ Mixtures in the Geological Sequestration fom 12 to 100º and up to 600 bar. *Geochim. Cosmochim. Acta* **2003,** *67*, 3015-3031.

66. Peng, D. Y.; Robinson, D. B. A New Two-Constant Equation of State. *Ind. Eng. Chem. Fundam.* **1976,** *15*, 59-64.

67. Wang, J.; Kalinichev, A. G.; Kirkpatrick, R. J. Effects of Substrate Structure and Composition on the Structure, Dynamics and Energetics of Water at Mineral Surfaces: A Molecular Dynamics Modeling Study. *Geochim. Cosmochim. Acta* **2006,** *70*, (3), 562-582.

68. Wang, J.; Kalinichev, A. G.; Kirkpatrick, R. J.; Cygan, R. T. Structure, Energetics and Dynamics of Water Adsorbed on the Muscovite (001) Surface: A Molecular Dynamics Simulation. *J. Phys. Chem. B* **2005,** *109*, 15893-15905.

69. Loganathan, N.; Kalinichev, A. G. On the Hydrogen Bonding Structure at the Aqueous Interface of Ammonium-Substituted-Mica: A Molecular Dynamics Simulation. *Z. Naturforsch., A: Phys. Sci.* **2013,** *68a*, 91-100.

70. Luzar, A.; Chandler, D. Hydrogen-bond Kinetics in Liquid Water. *Nature* **1996**, *379*, 55-57.

71. Chowdhuri, S.; Chandra, A. Dynamics of Halide Ion-Water Hydrogen Bonds in Aqueous Solutions: Dependence on Ion Size and Temperature. *J. Phys. Chem. B* **2006**, *110*, 9674-9680.

72. Luzar, A. Resolving the Hydrogen Bond Dynamics Conundrum. *J. Chem. Phys*. **2000**, *113*, 10663.

73. Iskrenova-Tchoukova, E.; Kalnichev, A. G.; Kirkpatrick, R. J. Metal Cation Complexation with Natural Organic Matter in Aqueous Solutions: Molecular Dynamics Simulations and Potentials of Mean Force. *Langmuir* **2010**, *26*, 15909-15919.

74. Dazas, B.; Lanson, B.; Breu, J.; Robert, J.-L.; Pelletier, M.; Ferrage, E. Smectite Fluorination and its Impact on Interlayer Water Content and Structure: A Way to Fine Tune the Hydrophilicity of Clay Surfaces. *Micro. Meso. Mat.* **2013,** *181*, 233-247.

75. Criscenti, L. J.; Cygan, R. T. Molecular Simulations of Carbon Dioxide and Water: Cation Solvation. *Environ. Sci. Technol.* **2013**, *47*, 87-94.

76. Ohtaki, H.; Radnai, T. Structure and Dynamics of Hydrated Ions. *Chem. Rev.* **1993,** *93*, 1157-1204.

77. Pouvreau, M.; Greathouse, J.A.; Cygan, R.T; Kalinichev, A.G. Structure of Hydrated Gibbsite and Brucite Edge Surfaces: DFT Results and Further Development of the ClayFF Classical Force Field with Metal-O-H Angle Bending Terms. *J. Phys. Chem. C* **2017**, *121*, 14457-14471.

**Table 1.** Mole fraction and fugacity coefficients of $H_2O$ and $CO_2$ in $H_2O$-saturated $CO_2$ for different $T$ and $P$ combinations used in this study obtained from Spycher et al.[65]

| $T$ (K) | $P$ (bar) | $x_{H2O}$ | $x_{CO2}$ | $f_{H2O}$ | $f_{CO2}$ |
|---|---|---|---|---|---|
| 323 | 90 | 0.0041 | 0.9959 | 0.231 | 0.654 |
| | 120 | 0.0055 | 0.9945 | 0.089 | 0.554 |
| | 150 | 0.0062 | 0.9938 | 0.055 | 0.481 |
| 348 | 90 | 0.0083 | 0.9917 | 0.374 | 0.732 |
| | 120 | 0.0085 | 0.9915 | 0.235 | 0.657 |
| | 150 | 0.0098 | 0.9902 | 0.147 | 0.594 |
| 368 | 90 | 0.0150 | 0.9850 | 0.453 | 0.778 |
| | 120 | 0.0141 | 0.9859 | 0.328 | 0.717 |
| | 150 | 0.0150 | 0.9850 | 0.234 | 0.664 |

**Table 2.** $CO_2$ mole fraction at stable interlayer distances for flexible and rigid structural -OH groups in comparison to results on montmorillonite.

| | Interlayer distance | *T* \ *P* | 90 bar | 120 bar | 150 bar |
|---|---|---|---|---|---|
| **Na – hectorite** | | 323 K | 0.058 | 0.058 | 0.062 |
| **(flex. –OH)** | Monolayer (12.2 Å) | 348 K | 0.047 | 0.045 | 0.041 |
| | | 368 K | 0.038 | 0.042 | 0.038 |
| | | 323 K | 0.0003 | 0.0003 | 0.0003 |
| | Bilayer (15.0 Å) | 348 K | 0.0002 | 0.0003 | 0.0002 |
| | | 368 K | 0.0002 | 0.0002 | 0.0003 |
| **Na – hectorite** | | 323 K | 0.180 | - | - |
| **(rigid -OH)** | Monolayer (12.5 Å) | 348 K | 0.142 | - | - |
| | | 368 K | 0.122 | - | - |
| | | 323 K | 0.035 | - | - |
| | Bilayer (15.5 Å) | 348 K | 0.031 | - | - |
| | | 368 K | 0.028 | - | - |
| **Na – hectorite experiments**[12] | | **323 K** | **0.140** | - | - |
| **Na – montmorillonite** | | | | | |
| | Monolayer (12.4 Å)[51] | 348 K | - | ~0.121 (125 bar) | - |
| | Monolayer (12.5 Å)[48] | 348 K | - | ~0.056 (125 bar) | - |
| | Monolayer (12.0 Å)[49] | 348 K | - | ~0.090 (130 bar) | - |
| | Monolayer (12.0 Å)[49] | 323 K | ~0.134 | - | - |
| | Bilayer (15.5 Å)[51] | 348 K | - | ~0.044 (125 bar) | - |
| | Bilayer (15.0 Å)[48] | 348 K | - | ~0.025 (125 bar) | - |
| | Bilayer (15.9 Å)[49] | 348 K | - | ~0.020 (130 bar) | - |
| | Bilayer (15.9 Å)[49] | 323 K | ~0.019 | - | - |

**Table 3.** Calculated intermittent and continuous residence times (ps) for the listed atomic pairs in the interlayers of Na-hectorite.

| $T$ (K) | basal spacing (Å) | $Na^+$-$O_{H2O}$ | $Na^+$-$O_b$ | $Na^+$-$O_{CO2}$ | $O_{H2O}$-$O_b$ | $O_b$-$O_{CO2}$ | $O_{H2O}$-$CO_2$ |
|---|---|---|---|---|---|---|---|
| | | | | $c(t)$ : $C(t)$ | | | |
| 323 | 12.2 (flex) | 594 : 48 | 538 : 18 | 8 : 6 | 582 : 38 | 57 : 35 | 59 : 8 |
| | 12.5 (rigid) | 609 : 57 | 529 : 19 | 12 : 8 | 571 : 41 | 61 : 34 | 57 : 10 |
| | 15.0 (flex) | 302 : 23 | 19 : 9 | - : - | 255 : 13 | - : - | - : - |
| | 15.4 (rigid) | 295 : 22 | - : - | 5 : 3 | 241 : 15 | 17 : 6 | 29 : 15 |
| 348 | 12.2 (flex) | 543 : 36 | 472 : 17 | 8 : 3 | 524 : 19 | 42 : 17 | 36 : 6 |
| | 12.5 (rigid) | 556 : 39 | 479 : 19 | 11 : 3 | 509 : 25 | 45 : 18 | 35 : 5 |
| | 15.0 (flex) | 245 : 11 | 20 : 6 | - : - | 207 : 8 | - : - | - : - |
| | 15.4 (rigid) | 231 : 19 | - : - | 5 : 4 | 203 : 13 | 18 : 5 | 27 : 14 |
| 368 | 12.2 (flex) | 503 : 27 | 404 : 14 | 7 : 3 | 477 : 14 | 29 : 6 | 39 : 5 |
| | 12.5 (rigid) | 509 : 25 | 411 : 15 | 10 : 4 | 471 : 12 | 22 : 6 | 35 : 7 |
| | 15.0 (flex) | 229 : 10 | 18 : 6 | - : - | 170 : 6 | - : - | - : - |
| | 15.4 (rigid) | 235 : 15 | - : - | 6 : 4 | 153 : 9 | 15 : 5 | 27 : 10 |

## FIGURE CAPTIONS

**Figure 1.** Average number of intercalated $CO_2$ and $H_2O$ molecules in the Na-hectorite interlayers per unit cell as functions of interlayer basal spacing at different combinations of simulated *T* and *P*. Color code: black – 323K; red – 348K; green – 368K. Figure d is for simulations at 90 bar using fixed structural -OH groups. The error bars show the 95% confidence level.

**Figure 2.** Computed immersion energies associated with intercalated $CO_2$ and $H_2O$ molecules in Na-hectorite interlayers as functions of interlayer basal spacing at different combinations of simulated *T* and *P*. Figure d is for simulations at 90 bars using fixed structural -OH groups. The circle in c) illustrates the shallow minimum at monolayer basal spacings.

**Figure 3.** Computed atomic density profiles of $O_b$ (dark blue vertical lines), $Na^+$ (orange), $O_{H2O}$ (red), $H_{H2O}$ (cyan), $O_{CO2}$ (green) and $C_{CO2}$ (violet) in Na-hectorite with flexible structural $OH^-$ groups as functions of distance from the basal clay surface at 90 bar for 3 different *T*. a)-c) are for monolayer basal spacings. d)-f) are for bilayer basal spacings.

**Figure 4.** Computed atomic density profiles of $O_b$ (dark blue vertical lines), $Na^+$ (orange), $O_{H2O}$ (red), $H_{H2O}$ (cyan), $O_{CO2}$ (green) and $C_{CO2}$ (violet) in simulations of Na-hectorite with rigid structural $OH^-$ groups as functions of distance from the basal clay surface at 90 bar for 3 different *T*. a)-c) are for monolayer basal spacings. d)-f) are for bilayer hydrate basal spacings.

**Figure 5.** Computed orientation distributions of intercalated $CO_2$ molecules in the interlayers oNa-hectorite at 323 K and 90 bar with flexible (flex) and rigid structural -OH

groups. Θ is the angle between the O-O vector of the $CO_2$ molecules and the normal to the hectorite basal surface. a) and b) are for monolayer basal spacings. c) and d) are for bilayer basal spacings.

**Figure 6.** Computed orientation distributions of $H_2O$ molecules intercalated in the interlayers Na-hectorite at 323 K (circles), 348 K (squares), 368 K (triangles) and 90 bar with flexible (flex) and rigid structural -OH groups. a) Dipole (black) and HH vector (red) at monolayer basal spacings with flexible -OH groups (12.2 Å). b) Dipole (black) and HH vector (red) at monolayer basal spacings with rigid -OH groups (12.5 Å). a) Dipole (black) and H-H (red) vectors at bilayer basal spacings with flexible -OH groups (15.0 Å). b) Dipole (black) and H-H (red) vectors at bilayer structure with rigid -OH groups

**Figure 7.** Computed PADDs of interlayer $Na^+$ ions and $CO_2$ and $H_2O$ molecules in Na-hectorite interlayers at monolayer basal spacings and 323 K and 90 bar with flexible and rigid -OH groups. a) $Na^+$ and $CO_2$ at the maximum $CO_2$ intercalation (12.2 Å) with flexible -OH groups; b) $Na^+$ and $CO_2$ at the maximum $CO_2$ intercalation (12.5 Å) with rigid -OH groups; c) $Na^+$ and $O_{H2O}$ and $H_{H2O}$ of $H_2O$ molecules at $z < 2.2$ Å at the maximum $CO_2$ intercalation (12.2 Å) with flexible -OH groups; d) $Na^+$ and $O_{H2O}$ and $H_{H2O}$ of $H_2O$ molecules at $z < 2.2$ Å at the maximum $CO_2$ intercalation with rigid -OH groups (12.5 Å). e) $Na^+$ and $O_{H2O}$ and $H_{H2O}$ of $H_2O$ molecules at $z > 2.2$ and $z < 3.2$ Å at the maximum $CO_2$ intercalation (12.2 Å) with flexible -OH groups; f) $Na^+$ and $O_{H2O}$ and $H_{H2O}$ of $H_2O$ molecules at $z > 2.2$ Å and $z < 3.6$ Å at the maximum $CO_2$ intercalation with rigid -OH groups (12.5 Å). Color code: $O_b$ – gray (dark and light), Si – yellow (dark and light), $Na^+$ – blue ($z < 2.8$ Å) and orange ($z > 2.8$ Å), $O_{CO2}$ – pink, $C_{CO2}$ –

green, $O_{H2O}$ – red, $H_{H2O}$ – cyan. Dark colors correspond to the $O_b$ and Si of one hectorite basal surface, and light colors correspond to those atoms of the opposite basal surface.

**Figure 8.** Computed PADDs of interlayer $Na^+$ ions and $CO_2$ and $H_2O$ molecules in Na-hectorite interlayers at bilayer basal spacings and 323 K and 90 bar with flexible and rigid -OH groups. a) $Na^+$, $O_{CO2}$, and $C_{CO2}$ of $CO_2$ with flexible -OH groups. b) $O_{CO2}$, and $C_{CO2}$ of $CO_2$ with rigid -OH groups. Color code: $O_b$ – gray (dark and light), Si – yellow (dark), $Na^+$ – blue ($z < 2.8$ Å) and orange ($z > 2.8$ Å), $O_{CO2}$ – pink, $C_{CO2}$ – green, $O_{H2O}$ – red, $H_{H2O}$ – cyan.

**FIGURES**

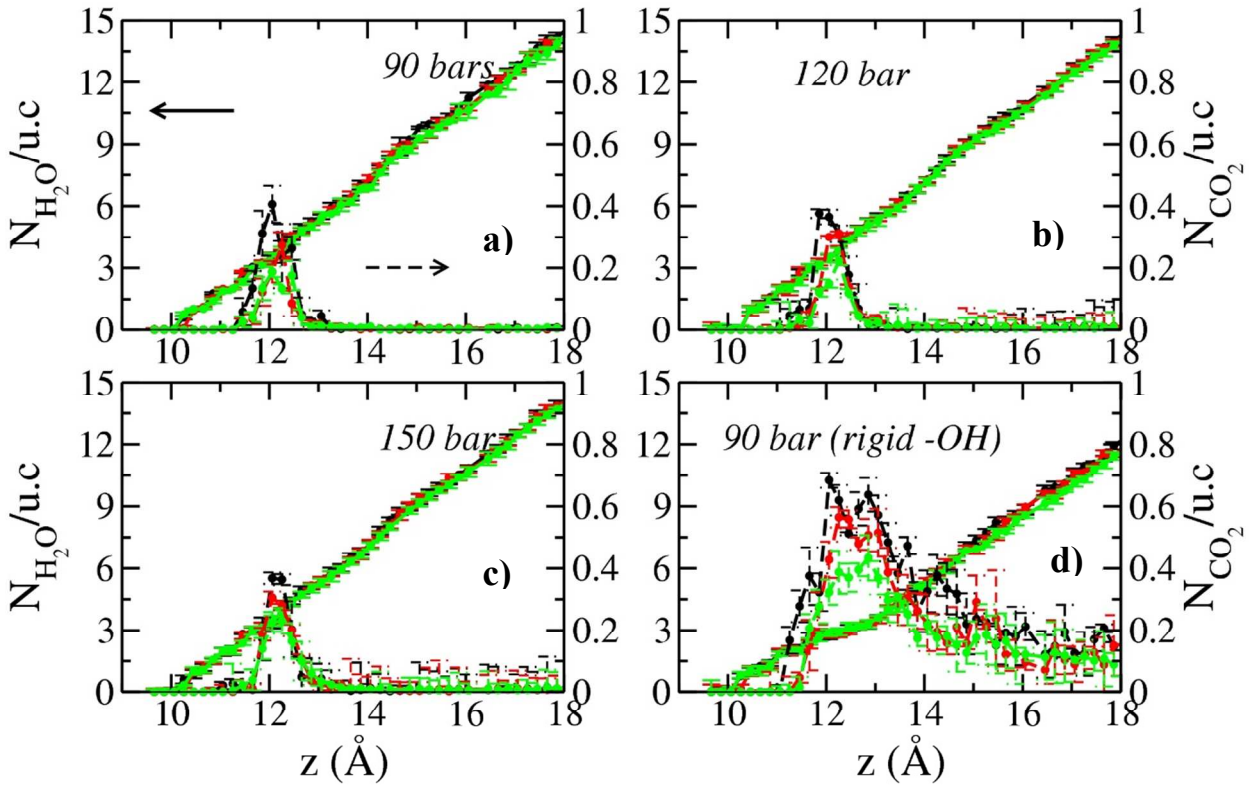


**Figure 1.** Average number of intercalated $CO_2$ and $H_2O$ molecules in the Na-hectorite interlayers per unit cell as functions of interlayer basal spacing at different combinations of simulated *T* and *P*. Note that the $CO_2$ data are expanded (see the right hand y axis) since a small number of $CO_2$ are present in the interlayer relative to the interlayer H2O at most conditions. Color code: black – 323K; red – 348K; green – 368K. Figure d is for simulations at 90 bar using fixed structural -OH groups. The error bars show the 95% confidence level.

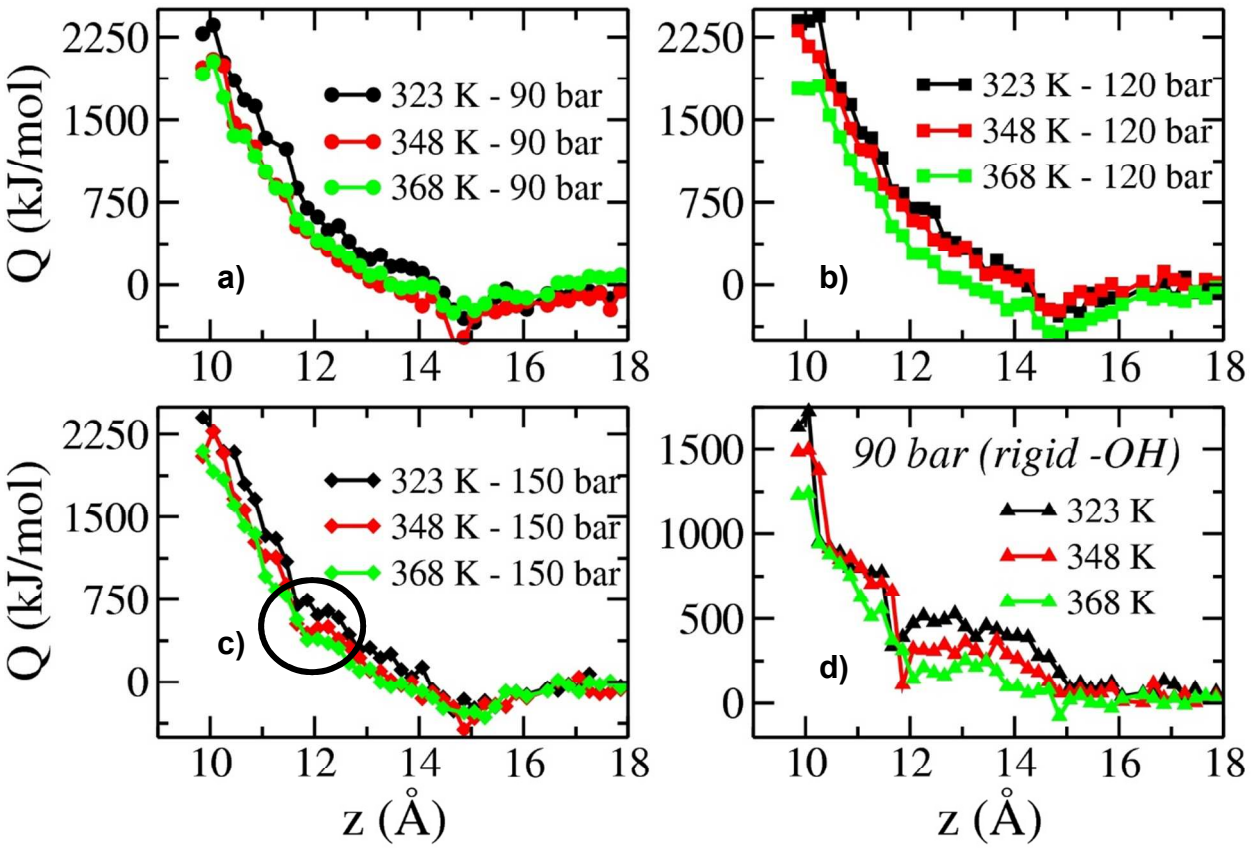


**Figure 2.** Computed immersion energies associated with intercalated $CO_2$ and $H_2O$ molecules in Na-hectorite interlayers as functions of interlayer basal spacing at different combinations of simulated *T* and *P*. Figure d is for simulations at 90 bars using fixed structural -OH groups. The circle in c) illustrates the shallow minimum at monolayer basal spacings.

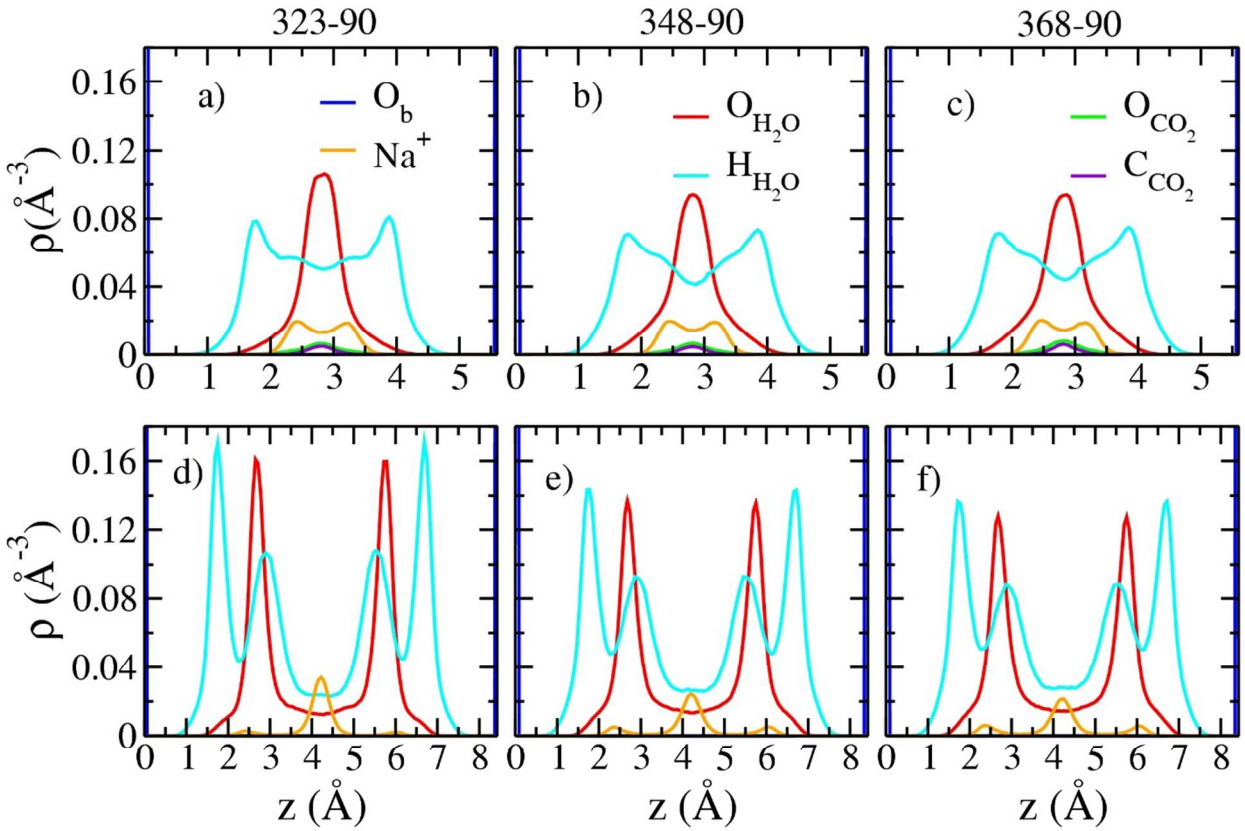


**Figure 3.** Computed atomic density profiles of $O_b$ (dark blue vertical lines), $Na^+$ (orange), $O_{H2O}$ (red), $H_{H2O}$ (cyan), $O_{CO2}$ (green) and $C_{CO2}$ (violet) in Na-hectorite with flexible structural $OH^-$ groups as functions of distance from the basal clay surface at 90 bar for 3 different *T*. a)-c) are for monolayer basal spacings. d)-f) are for bilayer basal spacings.

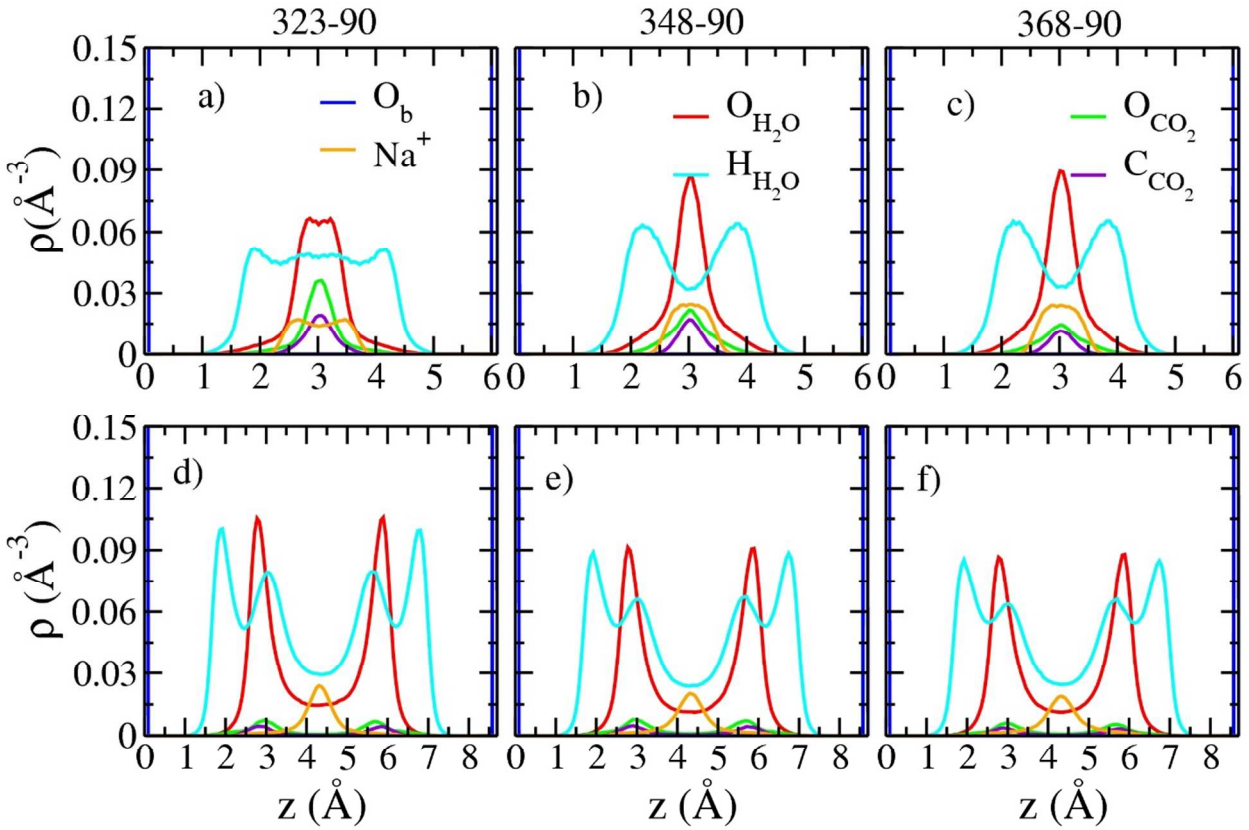


**Figure 4.** Computed atomic density profiles of $O_b$ (dark blue vertical lines), $Na^+$ (orange), $O_{H2O}$ (red), $H_{H2O}$ (cyan), $O_{CO2}$ (green) and $C_{CO2}$ (violet) in simulations of Na-hectorite with rigid structural $OH^-$ groups as functions of distance from the basal clay surface at 90 bar for 3 different *T*. a)-c) are for monolayer basal spacings. d)-f) are for bilayer hydrate basal spacings.

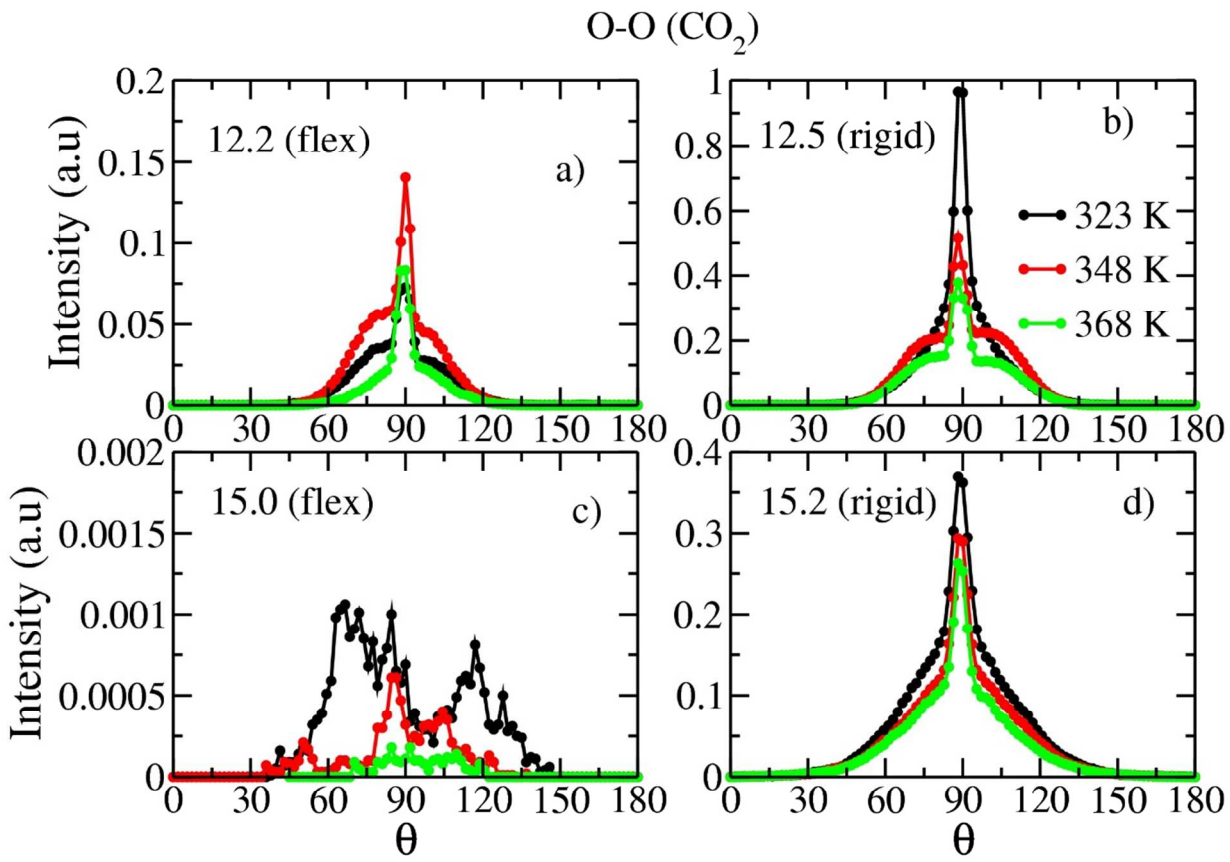


**Figure 5.** Computed orientation distributions of intercalated $CO_2$ molecules in the interlayers Na-hectorite at 323 K and 90 bar with flexible (flex) and rigid structural -OH groups. Θ is the angle between the O-O vector of the $CO_2$ molecules and the normal to the hectorite basal surface. a) and b) are for monolayer basal spacings. c) and d) are for bilayer basal spacings.

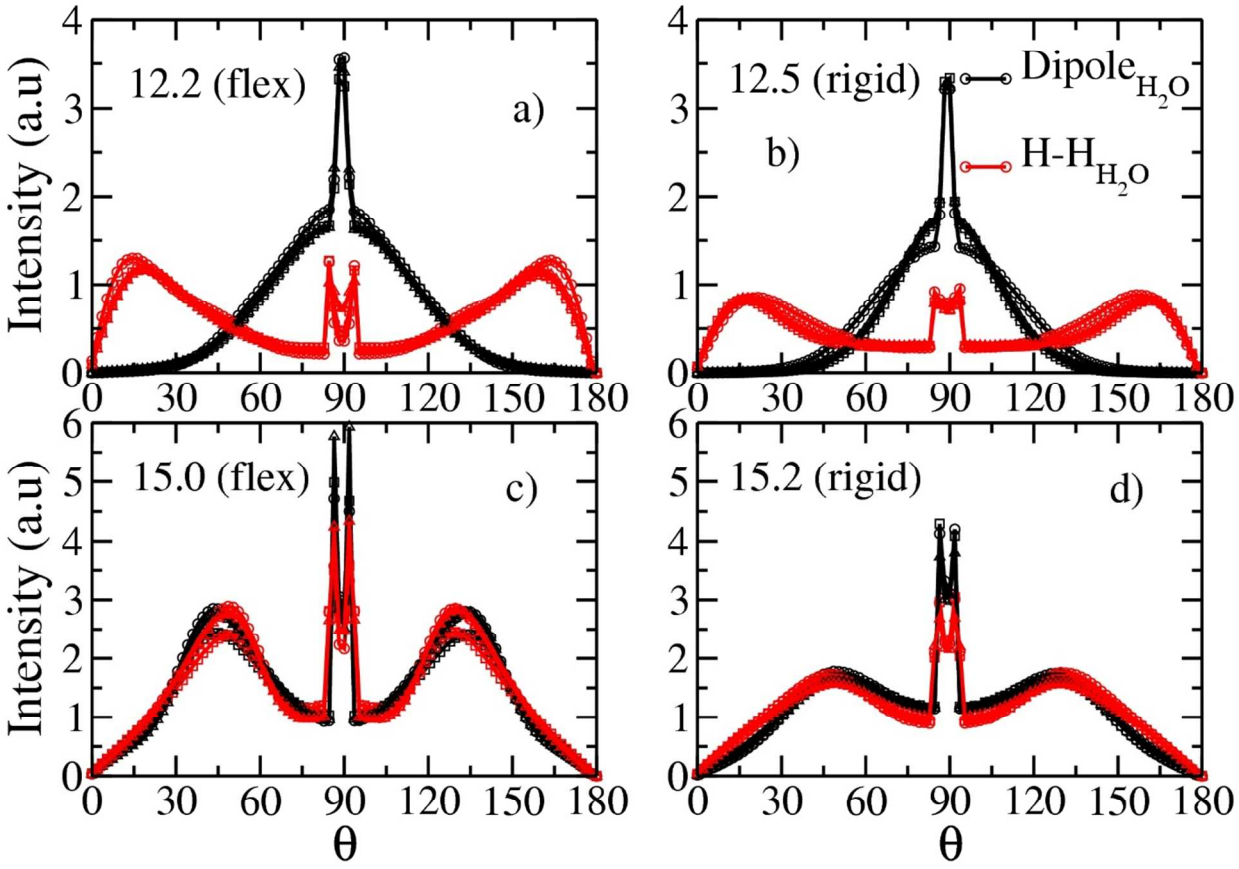


**Figure 6.** Computed orientation distributions of $H_2O$ molecules intercalated in the interlayers Na-hectorite at 323 K (circles), 348 K (squares), 368 K (triangles) and 90 bar with flexible (flex) and rigid structural -OH groups. a) Dipole (black) and HH vector (red) at monolayer basal spacings with flexible -OH groups (12.2 Å). b) Dipole (black) and HH vector (red) at monolayer basal spacings with rigid -OH groups (12.5 Å). a) Dipole (black) and H-H (red) vectors at bilayer basal spacings with flexible -OH groups (15.0 Å). b) Dipole (black) and H-H (red) vectors at bilayer structure with rigid -OH groups (15.2 Å).

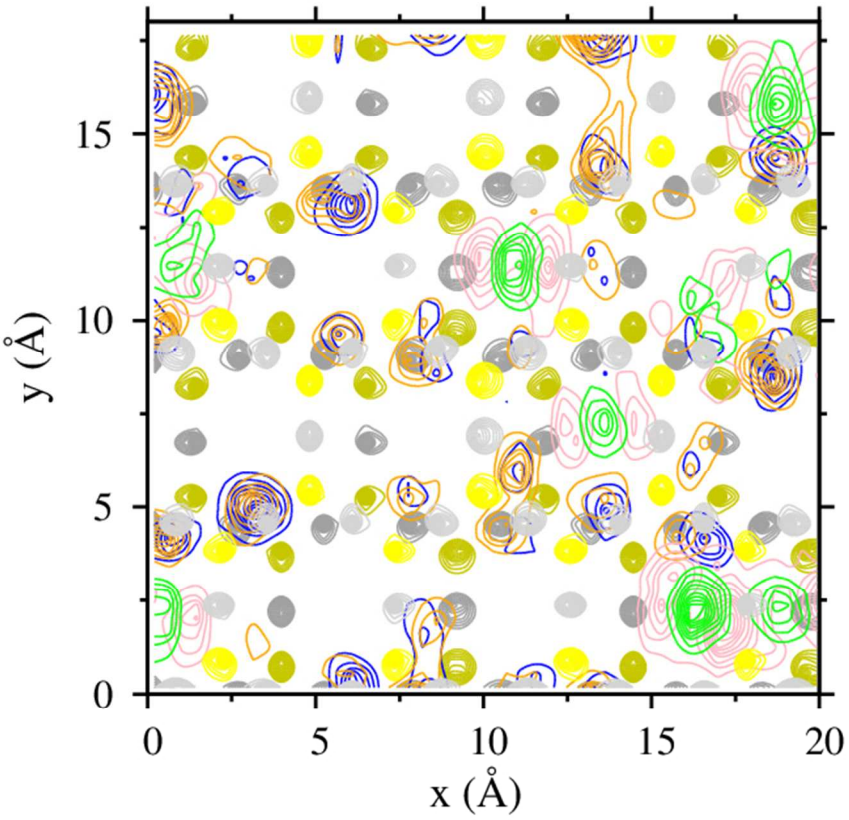


a)

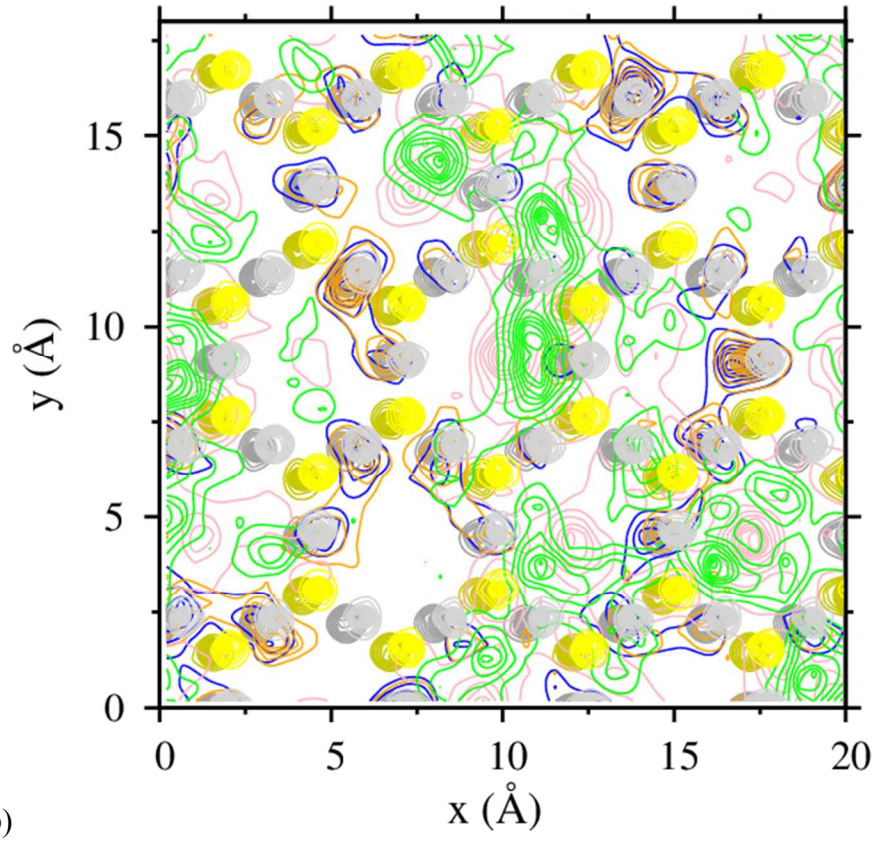


b)

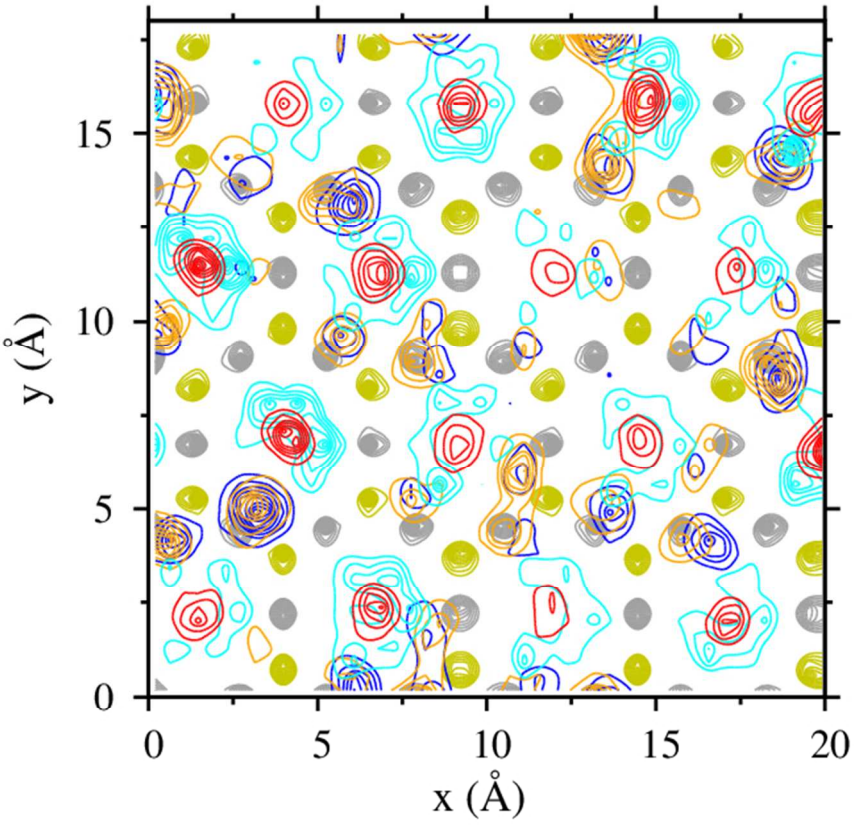


c)

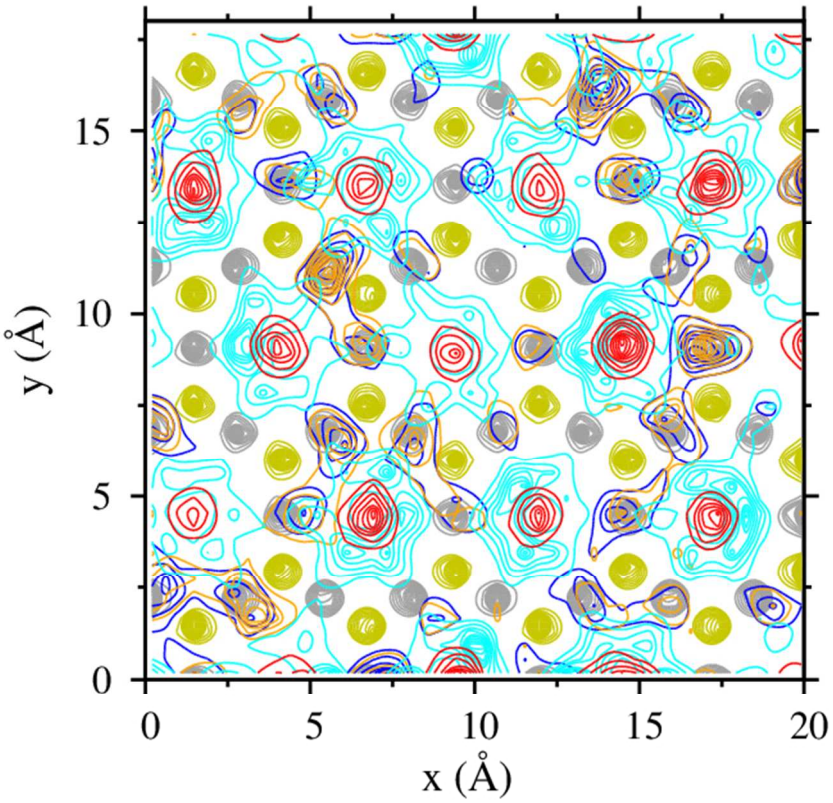


d)

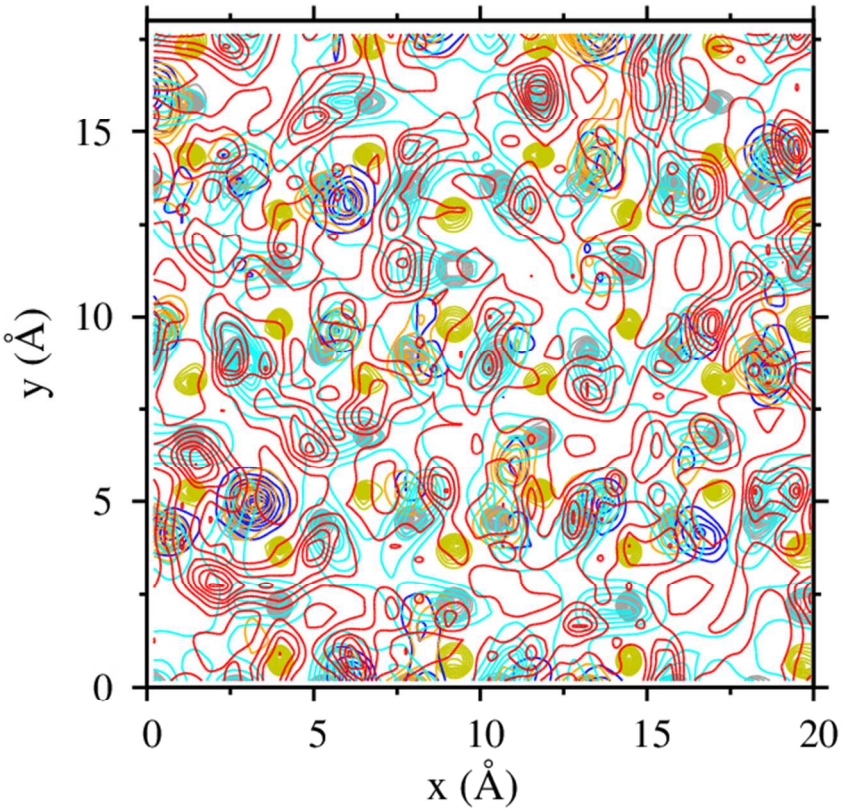


e)

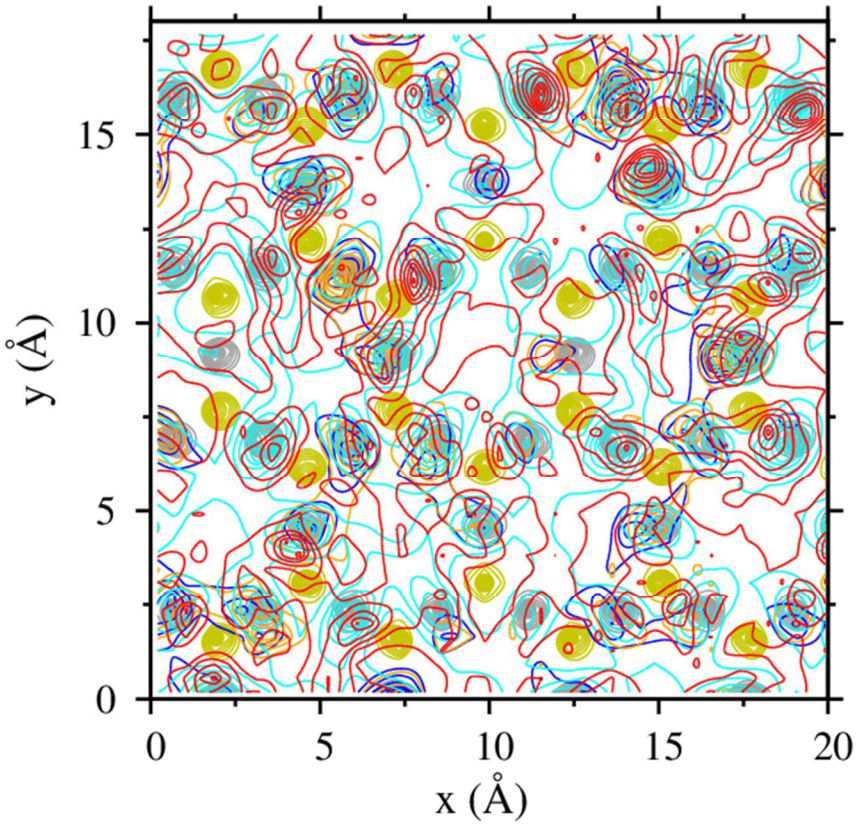


f)

**Figure 7.** Computed PADDs of interlayer $Na^+$ ions and $CO_2$ and $H_2O$ molecules in Na-hectorite interlayers at monolayer basal spacings and 323 K and 90 bar with flexible and rigid -OH groups. a) $Na^+$ and $CO_2$ at the maximum $CO_2$ intercalation (12.2 Å) with flexible -OH groups; b) $Na^+$ and $CO_2$ at the maximum $CO_2$ intercalation (12.5 Å) with rigid -OH groups; c) $Na^+$ and $O_{H2O}$ and $H_{H2O}$ of $H_2O$ molecules at $z < 2.2$ Å at the maximum $CO_2$ intercalation (12.2 Å) with flexible -OH groups; d) $Na^+$ and $O_{H2O}$ and $H_{H2O}$ of $H_2O$ molecules at $z < 2.2$ Å at the maximum $CO_2$ intercalation with rigid -OH groups (12.5 Å). e) $Na^+$ and $O_{H2O}$ and $H_{H2O}$ of $H_2O$ molecules at $z > 2.2$ and $z < 3.2$ Å at the maximum $CO_2$ intercalation (12.2 Å) with flexible -OH groups; f) $Na^+$ and $O_{H2O}$ and $H_{H2O}$ of $H_2O$ molecules at $z > 2.2$ Å and $z < 3.6$ Å at the maximum $CO_2$ intercalation with rigid -OH groups (12.5 Å). Color code: $O_b$ – gray (dark and light), Si – yellow

(dark and light), $Na^+$ – blue (z < 2.8 Å) and orange (z > 2.8 Å), $O_{CO2}$ – pink, $C_{CO2}$ – green, $O_{H2O}$ – red, $H_{H2O}$ – cyan. Dark colors correspond to the $O_b$ and Si of one hectorite basal surface, and light colors correspond to those atoms of the opposite basal surface.

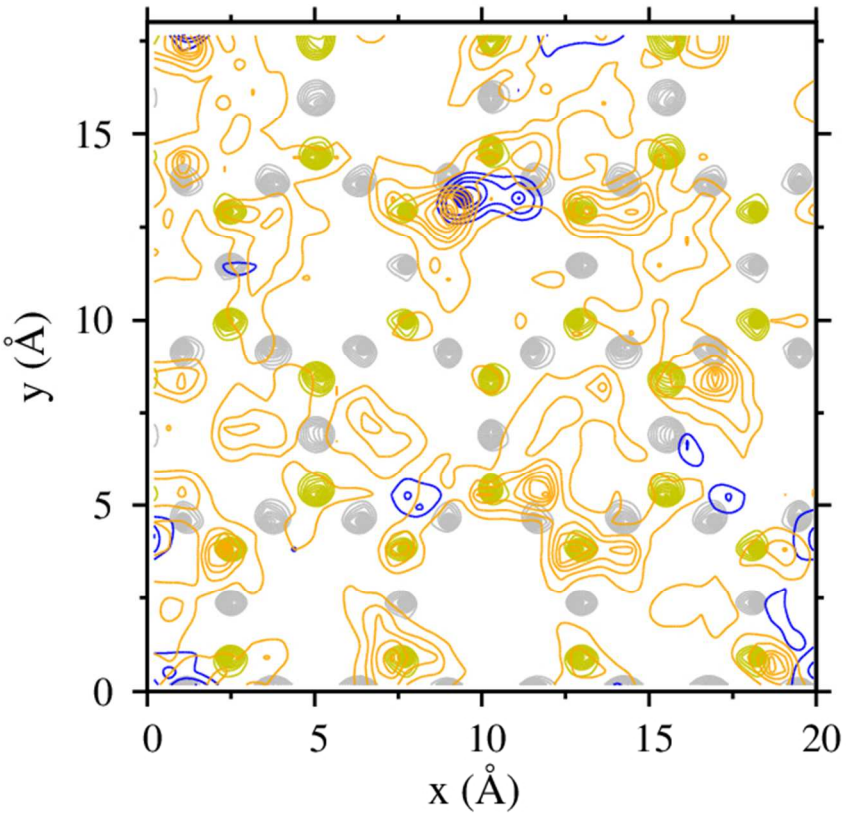


a)

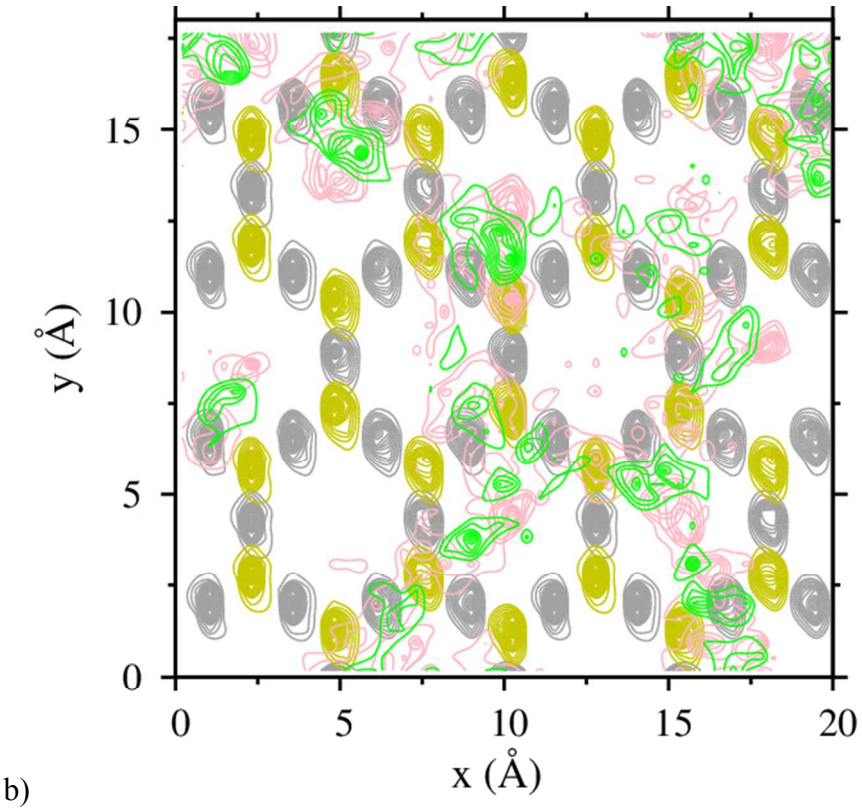


b)

**Figure 8.** Computed PADDs of interlayer $Na^+$ ions and $CO_2$ and $H_2O$ molecules in Na-hectorite interlayers at bilayer basal spacings and 323 K and 90 bar with flexible and rigid -OH groups. a) $Na^+$, $O_{CO2}$, and $C_{CO2}$ of $CO_2$ with flexible -OH groups. b) $O_{CO2}$, and $C_{CO2}$ of $CO_2$ with rigid -OH groups. Color code: $O_b$ – gray (dark and light), Si – yellow (dark), $Na^+$ – blue ($z < 2.8$ Å) and orange ($z > 2.8$ Å), $O_{CO2}$ – pink, $C_{CO2}$ – green, $O_{H2O}$ – red, $H_{H2O}$ – cyan.

## Table of Contents (TOC) Graphic